Unraveling a Few Mysteries of Melanin Polymerization:
Structure and Kinetics of Formation

A thesis submitted towards partial fulfillment of the requirements of
BS-MS Dual Degree Program

by

ARYA THAMPI

20101019

Indian Institute of Science Education and Research Pune

Under the guidance of

Dr. MRINALINI J. PURANIK

Associate Professor

Department of Chemistry

Indian Institute of Science Education and Research Pune- 411008

Certificate

This is to certify that this dissertation entitled "**Unraveling a few mysteries of melanin polymerization: Structure and kinetics of formation**" towards the partial fulfillment of the BSMS dual degree programme at the Indian Institute of Science Education and Research, Pune represents original research carried out by Arya Thampi at IISER Pune under the supervision of Dr. Mrinalini Puranik, Associate Professor, Department of Chemistry, IISER Pune during the academic year 2014-2015.

Date: *22 March 2015*
Place: *Pune*

Dr. Mrinalini Puranik
Associate Professor
Department of Chemistry
IISER Pune

Declaration

I hereby declare that the matter embodied in the report entitled "**Unraveling a few mysteries of melanin polymerization: Structure and kinetics of formation**" are the results of the investigations carried out by me at the Department of Chemistry, Indian Institute of Science Education and Research, Pune, under the supervision of Dr. Mrinalini J. Puranik and the same has not been submitted elsewhere for any other degree.

Date: 25th March 2015

Place: Pune

Arya Thampi

Acknowledgements

The conception and survival of this thesis was ignited and flamed by my advisor, Dr. Mrinalini Puranik. She taught me how to deal with scientific questions that evolve during the course of enquiry. My notion of scientific thinking was challenged and molded under her guidance, which was one of the biggest intellectual progresses I made in the past one year. As my guide and mentor, I am truly indebted towards her, for the unfailing patience and support, and the wonderful experience of working with her.

My thesis would have been impossible without the guidance and comradeship of Sayan. From doing experiments together to having discussions (which involved quite a lot of arguing) and clearing my doubts (invariant of the length and amount of silliness in them at times), he was a fantastic senior to work with. I can never be thankful enough to the wonderful members of the Puranik lab, Shahila who is like an elder sister to me, Vishakha whose suggestions helped me a lot (in science and otherwise), Yashwant who filled the lab with his songs, Prashanth who did the same with his laughter, Anil who reminded all of us when the time for a meal or chai was up, and Sudeb for his unrelenting smile that would lift anyone's mood instantly, all of which made the lab an amazing place to work.

For having been there during difficult times to shed me the light of a smile, I fondly thank Sangamesh. For bearing with my little mischiefs between the last two summers, and for being a very understanding friend to me, I thank Siddhartha.

Last, but not the least, I would like to acknowledge my family for believing in me and what I do.

Dedicated to Achan and Amma

Table of contents

List of figures

List of tables

Abstract

Melanin is a very widely studied biopolymer, which gives colour to our eyes, skin, hair etc and whose complex structural hierarchy has puzzled researchers over the past century.[1] The biogenesis pathway of melanin had been investigated previously and found that the enzyme tyrosinase has a crucial role in the oxidation of precursors (tyrosine and 3,4-dihydroxyphenylalanine) that facilitates further oxidation to the indolic species of dihydroxyindole (DHI) and dihydroxyindole-2-carboxylic acid (DHICA), which take part in polymerization.[2] Though a general mechanism for consecutively produced reactants in this polymerization pathway was proposed back in 1926[3], kinetics is not entirely known yet. The current project aims to investigate the kinetics of melanin polymerization from the precursor molecule, 3,4-dihydroxyphenylalanine (DOPA), in the presence and absence of tyrosinase using spectroscopic methods. Due to the broad and interfering absorption spectra of melanin and intermediates[4], the obtained kinetics of several intermediates from absorbance data wrongly estimates the original value. We have measured kinetics using resonance Raman (RR) spectroscopy which probes molecular vibrational energy levels and thus is intrinsically of a higher spectral resolution than that of absorption spectroscopy. In the current study a novel reduced reaction model arises from RR derived kinetics which sheds considerable amount of light on the current understanding of melanin synthesis pathway. The rate constants obtained by using the above mentioned models of the kinetics of various intermediates and products, with and without the enzyme, are discussed with their significance. A major finding in this work is the evidence for the regulatory action of the enzyme tyrosinase on the heterogeneity of the polymers formed. The latter part of the project looks at the vibrational spectroscopy of various cell types with and without melanin.

Introduction

Melanin is one of the most studied biological polymers that gives skin, hair, and eyes their natural colour. There are primarily three types of melanin: Eumelanin (present in humans, black), pheomelanin (present in various animal species, yellow-brown in colour) and neuromelanin (pigmented neurons in the substantia nigra region of brain[5]). Melanin is responsible for vital functions such as cross-linking of proteins and hence improves the strength of protein structures and prevents degradation[6,7], photoprotection[8], thermal regulation[9] of cells etc. Melanin biosynthesis is a complex pathway (Figure. I) that takes place within melanosomes, specialized membrane-bound organelles inside a class of dendritic cell type called melanocytes.[10] Melanocytes are located in various parts of body e.g. bottom layer of epidermis, middle layer of eye, meninges and the heart.[11] Melanosomes are transferred from melanocyte dendrites to surrounding keratinocytes, upon maturation and growth.[12]
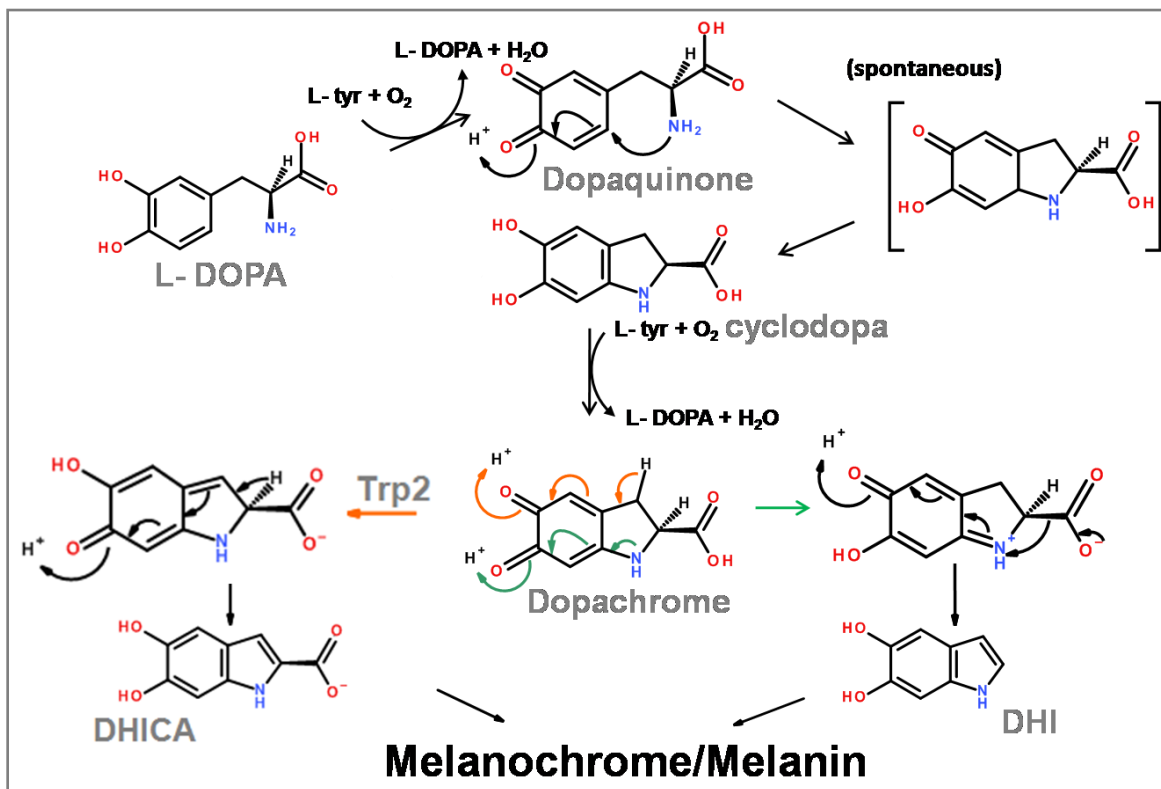
Figure I. Biosynthetic pathway of melanogenesis.[13]

Eumelanin is composed of aggregated oligomeric and polymeric species of indolic monomers 5,6-dihydroxyindole (DHI), 5,6-dihydroxyindole-2-carboxy acid(DHICA) and their various redox forms.[3] A hierarchical structure formation of melanin polymerization was proposed in some earlier reviews.[14] In the biosynthesis pathway of melanin, various reaction intermediates have been isolated and identified using spectroscopic and various other characterization during the course of the reaction. The biological precursors of melanin, L-tyrosine and 3,4-dihydroxy-L-phenylalanine are oxidized in the presence of the enzyme tyrosinase, which is a diphenolic hydroxylase, and gives rise to dopaquinone and further to dopachrome, which spontaneously reduces to 5,6-dihydroxyindole (DHI). Dopachrome can also undergo reduction in the presence of dopachrome oxidase, which converts it to 5,6-dihydroxyindole-2-carboxylic acid (DHICA).[15] DHI and DHICA undergo polymerization to form melanin polymer, termed as melanochrome. Melanochrome is the soluble, non-aggregate form of melanin polymers with short chain length.[16]

The monomers are proposed to cross-link to form planar sheets, stacked via aromatic pi-interactions and with varying conjugation length.[17] The chemical characteristics of melanin polymers vary over a large range and this makes understanding its biophysical properties extremely challenging. Understanding the structure and kinetics of formation of melanin is one of the yet unresolved problems and it is one of the few bio-polymers whose structure and functions are not yet fully unveiled. Research in the field of melanin has taken various leads till date. While a several of them focus on the semiconducting, electronic properties of melanin,[18] others look for at the photophysical characteristics of melanin using spectroscopy as a tool.

Melanization has been shown to consist of two distinct processes: polymerization of melanochrome and aggregation of the formed melanin polymers.[17] Upon the addition of the precursor units to the system, it is allowed to undergo self-oxidation and thus, polymerization is facilitated. In the absence of enzymes such as tyrosinase, this step continues to happen for a few days in bulk. This constitutes the polymerization stage. As a result of polymerization, the individual polymeric units are now closer to each other and this may result in chain entanglement. This improves the Van der Waal's

interaction between the polymeric units and thus they come closer and start aggregating. This typically takes longer than a few days, in the absence of an enzyme. This is the process of aggregation. The timescales for the same processes are different for the enzyme and we also see stabilization of certain intermediates in the presence of the enzyme.

The kinetics of formation of insoluble black melanin aggregates had been followed by Dynamic Light Scattering (DLS) and Small-Angle Neutron Scattering (SANS) before, in the presence of crowding agents such as polyvinyl alcohol.[17] Small Angle Neutron Scattering (SANS) and Small Angle X-ray Scattering (SAXS) techniques were used to observe the formation of small aggregates of melanin induced by the addition of copper ions.[17] One of the aims of this project was to delineate these two processes by Raman spectroscopy. However, looking at the kinetics of formation of particles based on size alone is an inconclusive way of narrating the melanin polymerization story at molecular level. Realizing this, we propose and demonstrate a novel way to follow melanization process by probing vibrational modes that are unique for a given molecular species. The current study began with looking at the absorption kinetics, Fourier Transform-Infra Red spectroscopy (FTIR) and resonance Raman spectroscopy of auto-oxidation and enzyme assisted polymerization of DOPA.

Bulk melanin is a dark pigment with a complex physical structure which is a challenge to look spectroscopically at. It has a very broad characteristic absorption spectrum which poses an upper limit to the structural information retrieved from it. The absorption spectra of intermediates such as dopachrome and DHI monomer have also been studied previously.[19] However, to conclusively develop a model for explaining the kinetics of melanisation, the rate of evolution of intermediates and formation polymers have to be experimentally determined. Absorption spectral profiles of the intermediates may lead to rather disingenuous conclusions, which are revealed in the present study by using resonance Raman (RR) spectroscopy. RR spectroscopy provides with more comprehensive information at structural level. Unlike electronic spectroscopy, vibrational spectroscopy probes changes in the bond strength of a specific vibrational mode, and thus increases intrinsically improve structural resolution. The presence of

many intermediates has overlapping absorption contribution and hence the kinetics obtained through absorption studies is over- or underestimated at times. These are refined by RR measurement which determines more accurate rates of decay and formation of various species *en route* melanin.

Following the research done in the late 1940's and 1950's by Mason[4,20] and others, the kinetics of melanin polymerization was first performed by time-dependent absorption spectroscopy. In the current project, melanin polymerization starting from the precursor, 3,4-dihydoxyphenylalanine (L-DOPA) was studied in the presence and absence of the enzyme tyrosinase which assists the formation of melanin in living organisms. The goal of following the kinetics of melanin formation is to elucidate the much debated intermediates and their associated rates of during melanin polymerization. The enzyme that regulates the biogenesis of melanin, tyrosinase, plays the crucial role of oxidization of tyrosine/DOPA to form dopaquinone in the biogenesis of melanin polymer. Thus, it is extremely important to assess the role of tyrosinase in the regulation of melanin polymerization. In this project, melanin polymerization kinetics is carefully studied in two cases: auto-oxidation (non-enzymatic) of DOPA and enzymatic oxidation of DOPA in the presence of tyrosinase.

Till this part of the work we resorted to synthetically produced melanin since the extraction of natural melanin is an intricate and complex process (purification of proteins, secondary structures etc is cumbersome) and the stability of the natural product is very low. But in the larger picture, the functionality of melanin is most vital in the natural context i.e. natural melanin should be looked into spectroscopically as well, by *in vivo* studies. Thus, the latter part of this thesis focuses on the imaging of various types of cells with and without melanin. In this part, several cell lines such primary human keratinocytes, primary human melanocytes, primary human melanocytes treated with tyrosine and polythiouracil (PTU), HaCaT cells and B-16 pigmented mouse cells were analyzed by using Raman spectroscopy as an imaging tool. Vibrational spectroscopic studies on various types of cells have been previously done.[21,22,23,24] The objective of this part of work was to look at the spatial-structural similarities and dissimilarities of various cell components, especially melanin, in different cell types.

Experimental section

1 Chemicals and instruments used

1.1 Chemicals

3,4-Dihydoxy-L-phenylalanine (Sigma Aldrich D9628-5G), Tyrosinase from mushroom (Sigma Aldrich T3824-25KU), Potassium bromide (KBr) (Sigma Aldrich 243418-100G), Tris base (Sigma Aldrich T1503-25G), Sodium phosphate dibasic (Na_2HPO_4) (Sigma Aldrich S3264) and Sodium phosphate monobasic (NaH_2PO_4) (Sigma Aldrich S3139). All chemicals were used directly without further purification.

1.2 Instruments

- UV- 2600 Shimadzu double beam spectrophotometer, Shimadzu Corporation
- Zetasizer Nano-2590, Malvern Instruments Ltd, Worcestershire, UK
- Thermo-Scientific Nicolet 6700 FT-IR
- Ti: sapphire source pumped by a Nd:YAG diode pumped laser (Indigo, Coherent Inc.) for resonance Raman spectroscopy
- CW 785 nm laser (Innovative Photonics Solutions) coupled to a Raman microscope, LabRAM HR800 (Horiba Jobin-Yvon SAS)

2 Sample preparation

2.1 DOPA-melanin samples prepared in the absence of enzyme

5 mM L-DOPA solutions were prepared in 2 mL of 50 mM Tris-HCl buffer at pH 7.4, in a 2 mL eppendorf and was kept open in ambient environment covered with aluminum foil till the date of experiment to facilitate air oxidation. Sample were made for the time points 00 hour, 06 hours, 18 hours, 24 hours, 36 hours, 48 hours, 60 hours, 72 hours, 96 hours, 120 hours, 126 hours, 138 hours, 144 hours, 156 hours, 168 hours, 180 hours and 192 hours.

2.2   DOPA-melanin samples prepared in the presence of the enzyme

200 µL of 4 mM L-DOPA solution was mixed with 200 µL of 20 µg/mL mushroom Tyrosinase solution, in a glass NMR tube. Both solutions were made in 40 mM phosphate buffer at pH 6.8. The buffer, solid DOPA and the tube were purged with Argon for 30 minutes. Recording of data (Absorption/Raman) was commenced immediately after the mixing of the reagents.

3   Absorption spectroscopic studies of kinetics of DOPA-melanin formation

DOPA-melanin samples prepared in the absence of the enzyme (section 2.1) were diluted 50 times with the same buffer while recording the absorption spectra. Three independent reactions were monitored using a UV- 2600 Shimadzu double beam spectrophotometer, Shimadzu Corporation in a 1 mL quartz cuvette with a path length of 10 mm. (Spectral range= 200-700 nm, Bandwidth= 2 nm, Scan speed= 120 nm/min, Data interval= 0.5 nm).

Absorption studies of DOPA-melanin samples prepared in the presence of the enzyme (section 2.2) were recorded continuously for 10 hours with a gap of approximately 10 minutes. The experiment was done in a glass NMR tube of height 10 cm and diameter 5 mm (Wilmad-LabGlass). (Spectral range= 200-700 nm, Bandwidth= 2 nm, Scan speed= 120 nm/min, Data interval= 0.5 nm).

4   Resonance Raman spectroscopic studies of kinetics of DOPA-melanin formation

4.1   Resonance Raman experimental details at 263 nm and 488 nm

Raman spectra of the samples prepared in the absence of enzyme (section 2.1) were recorded at 261 nm, while the sample was spun along its axis in a quartz tube, with an exposure time of 1 minute. One sample was recorded for a period of 10 cycles and the average spectrum was processed. Controls were also recorded with the same constraints. Two independent sets of this experiment were performed. The excitation line was produced as third harmonic of a Ti:sapphire source pumped by a Nd:YAG diode pumped laser (Indigo, Coherent Inc.). The output was of 25 ns pulse width and 1

KHz repetition rate. Typical power on sample was ~ 600 μW. The Raman scattered light is collected and dispersed through a monochromator (Jobin-Yvon) of 1.25 m focal length and equipped with a 3600 grooves/mm holographic grating to focus on liquid N_2 cooled charge couple device (CCD) camera (Jobin-Yvon). Resolution of the detection system was ~ 2 cm^{-1}.

The kinetics of the samples prepared with enzyme was recorded at 263 nm and 488 nm laser excitation. At 263 nm, the Raman spectra of the sample was recorded for the first 700 minutes with an interval of 15-20 minutes and then later with at 60 minutes time interval, at 263 nm. The exposure time was set to be one minute and each time point spectrum was averaged over 15 cycles. Controls were also recorded with the same constraints. The 263 nm excitation laser and detection system is same as described above.

The 488 nm excited spectra is obtained by using a CW argon laser (Spectra-Physics) coupled to a Raman microscope, LabRAM HR800 (Horiba Jobin-Yvon SAS). The sample is put in a glass NMR tube and 20x objective was used for collection. A grating with 600 grooves/mm density and a liquid N_2 cooled CCD was used as detector. Power on sample was ~ 8-10 mW.

4.2   Spectral processing of Resonance Raman data

For both of the above mentioned Raman spectroscopy experiments, spectral processing was done in Origin 7.0 (OriginLab Corporation) and Labspec 5.64.15 (Jobin Yvon, France) as follows. The spectral average was calculated over a definite number of cycles, after which cosmic ray spikes were removed. Respective buffers were subtracted from each spectrum since buffer has a very broad band around 1645 cm^{-1}. After buffer subtraction, spectrum of blank quartz tube was subtracted from it. For the fitting of bands in order to look at absolute spectral intensity, baseline subtraction was done. In order to analyze the spectra without any monomer contribution, the monomer spectrum was also subtracted. All spectra were normalized with respect to the count of dimethylformamide recorded before and after each sample as an external intensity standard. Raman bands were fitted using Lorentzian line shape. The normalized area under the curve was used as intensity and was plotted against time.

The Raman data obtained at 488 nm was baseline subtracted in LabSpec using a polynomial function since the sample exhibits fluorescence at this wavelength, and thus produces an intense background signal.

5 Dynamic Light scattering spectroscopy of DOPA-melanin in the absence of enzyme

5 mM L-DOPA solutions were prepared in 2 mL of 50 mM Tris-HCl buffer at pH 7.4, in a 2 mL eppendorf and was kept open till the date of experiment to facilitate air oxidation. Samples were made for the time points 48 hours, 72 hours, 96 hours, 120 hours and 144 hours. The experiment was done using Zetasizer Nano-2590, Malvern Instruments Ltd, Worcestershire, UK, in 3 mL polystyrene cuvette with 10 mm path length.

6 Fourier Transform Infra-Red spectroscopy of DOPA-melanin in the absence of enzyme

5 mM L-DOPA solutions were prepared in 2 mL of 50 mM Tris-HCl buffer at pH 7.4, in a 2 mL eppendorf and was kept open till the date of experiment to facilitate air oxidation. As soon as a sample reached its time point, it was precipitated by using methanol in the ratio 1:25 (e.g. for the 24 hours sample, it was precipitated with methanol 24 hours after the preparation of the sample). After giving methanol wash for 2-3 times, the samples were dried in vacuum overnight. The powdered samples were mixed with potassium bromide (1:10 ratio by weight) to make solid pellets for the measurement of FT-IR spectra. All FT-IR measurements were done using Thermo-Scientific Nicolet 6700 FT-IR.

7 Micro-Raman spectroscopy of different types of skin cells

The instrument used was a CW 785 nm laser (Innovative Photonics Solutions) coupled to a Raman microscope, LabRAM HR800 (Horiba Jobin-Yvon SAS). A grating with 600 grooves/mm density and a liquid N_2 cooled CCD was used as detector. Laser power on sample was set at 25-30 mW. and samples were measured using a 60x water immersion objective. The cell fixing and imaging protocol is as given below.

A few thousand cells were fixed on 0.01 % poly-lysine coated quartz slides and were incubated at 37°C overnight. The cells grew by the next day and were fixed using chilled methanol at -20°C on the slide. 1 mL of 10 nM PBS buffer was added to the cells for rehydration before the imaging. ~200 ml of MiliQ water was added every 45 minutes to keep the cells hydrated and not phosphate salt to not get precipitated. After each cell being located, signal was monitored with 20 seconds exposure at continuous display mode with different z-values. Spectral recording was commenced after the optimization of the z-value. Confocal pinhole was normally kept at 200 or 300 µm and slit was set at 100-200 µm. A map of 10x10 array (100 points) was recorded from a cell with 60 seconds exposure time at each point. Background spectrum (signal from outside cell) is recorded during each Raman map. This signal is subtracted from all spectra recorded from the inside of the cell. The cell types used were primary human keratinocytes, primary human melanocytes, primary human melanocytes treated with tyrosine and polythiouracil and HaCaT cells. The cells were obtained from the lab of Dr. Rajesh Gokhale, IGIB, Delhi.

Results

8 Investigation of DOPA-melanin formation using absorption spectroscopy

8.1 Absorption kinetics of DOPA-melanin formation in the absence of enzyme (auto-oxidation)

Figure 8.1.1 shows the absorption kinetics of auto-oxidation of 3,4-dihydroxyphenylalanine (L-DOPA , used henceforth as DOPA) in the absence of tyrosinase, in 50 mM Tris-HCl buffer at pH 7.4. The reaction was followed from 00 hours to 199 hours. The precursor (DOPA) peak at 280nm was seen throughout the reaction, which means that the indole skeleton of consecutively formed components remains intact during melanin polymerization. It was seen that overall absorption in the 320-500 nm region increases over time. This increase in the slope of absorption spectrum between 0 hour and 192 hours is more distinctly shown in the inset. An intermediate between the monomer and the insoluble melanin polymer is termed as melanochrome, which is at a non-aggregate stage of polymerization. Melanochrome formation has been previously studied at 540 nm, but the current study finds this inadequate and hence melanochrome absorption is monitored at 363 nm (discussed later) as shown in Figure 8.1.2.

The kinetics was fit to a reduced model that was developed during this work, which is discussed later. The fit to experimental data for the kinetics of formation of melanochrome is as shown in Figure 8.1.2.
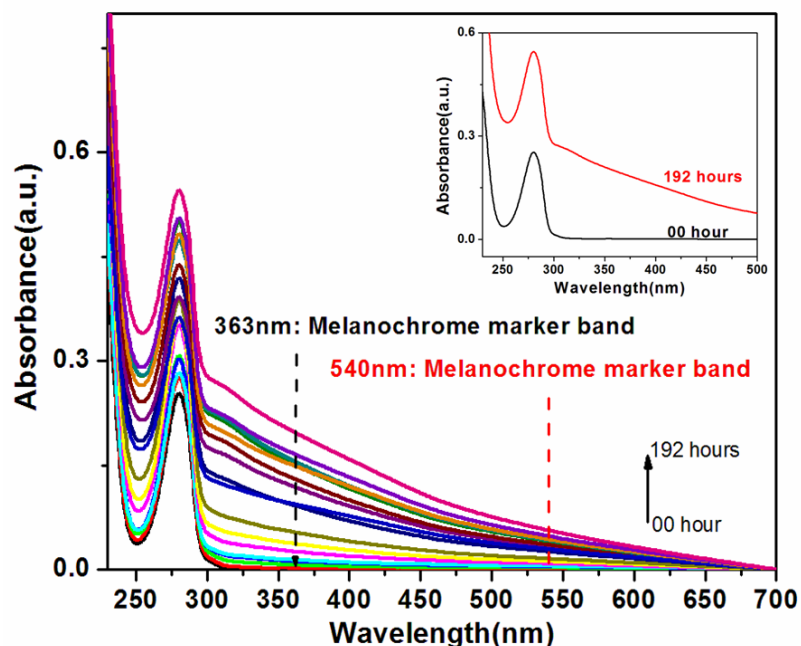
Figure 8.1.1 Absorption kinetics of DOPA-melanin in the absence of enzyme, in 50 mM Tris-HCl buffer at pH 7.4. Inset shows the absorption spectra at 0 hour and 192 hours. This experiment has been reproduced from the doctoral thesis of my colleague Sayan Mondal with permission.

$$y = a + k_M * t$$

| a | -0.02091 |
| k_M | 0.0014 |
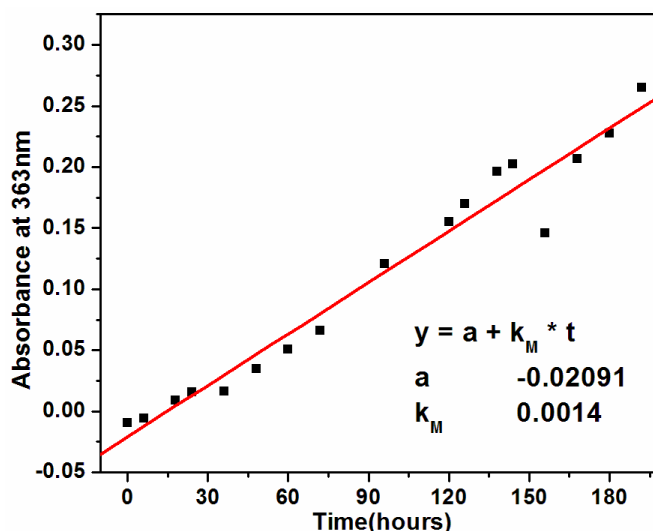
Figure 8.1.2 Absorption kinetics of melanochrome formation at 363 nm from 0 hour to 192 hours of the reaction. Fitting parameters and equation are shown. Abbreviations: k_M: Rate of formation of melanochrome, t: time, a: additive constant.

8.2 Absorption kinetics of DOPA-melanin formation in the presence of enzyme

Absorption kinetics of enzymatic oxidation of DOPA was monitored in the presence of the enzyme, mushroom tyrosinase up to 700 minutes of the reaction in 40 mM phosphate buffer at pH 6.8. Apart from the 280nm band of the precursor DOPA, two distinct bands were seen at 305 nm and 480 nm which belong to an intermediate, dopachrome (discussed later). Kinetics was followed at a concentration that was decided upon investigating kinetics at multiple concentrations. The absorption kinetics done with 2 mM DOPA and 10 µg/mL tyrosinase in 40 mM phosphate buffer at pH 6.8 is shown in Figure 8.2.1.
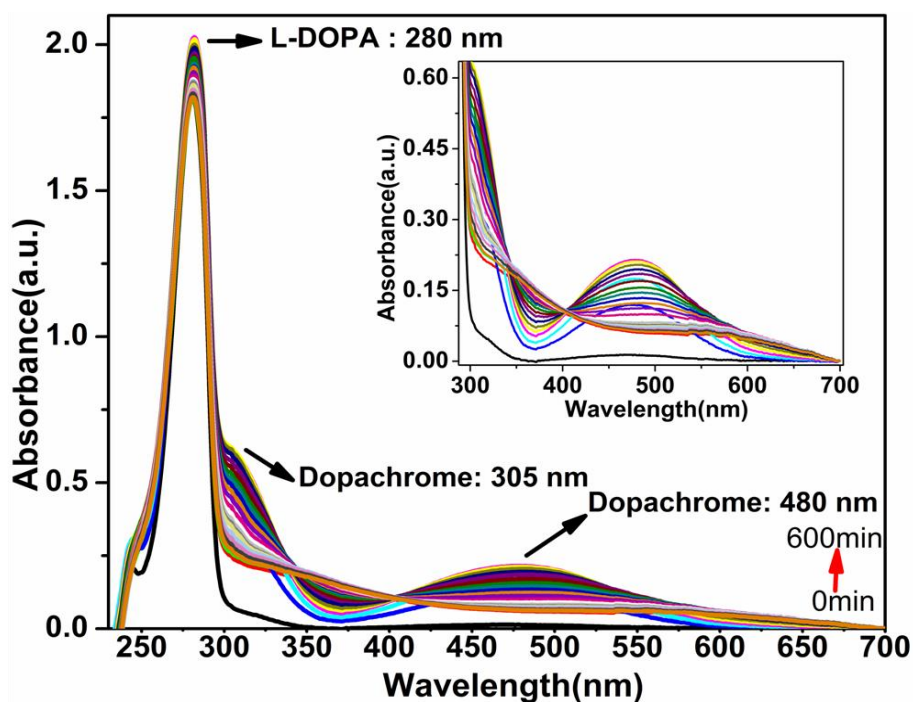
Figure 8.2.1 Absorption kinetics of DOPA-melanin in the presence of enzyme, in 40 mM phosphate buffer at pH 6.8 from 0 minute to 600 minutes of the reaction. Inset shows the enlarged region 300-700 nm. The absorption maxima for DOPA and dopachrome are marked.
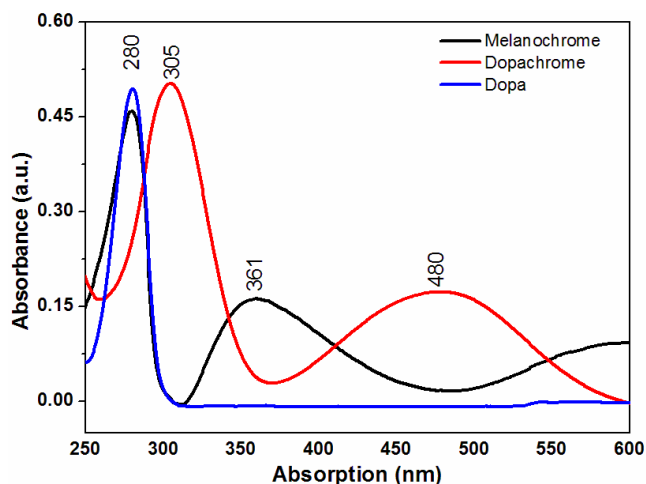
Figure 8.2.2 Absorption spectra of DOPA (blue), dopachrome (red) and melanochrome (black) in phosphate buffer at pH 6.8 and the corresponding λ_{max} values are marked. All spectra are obtained from the enzymatic oxidation reaction of DOPA.
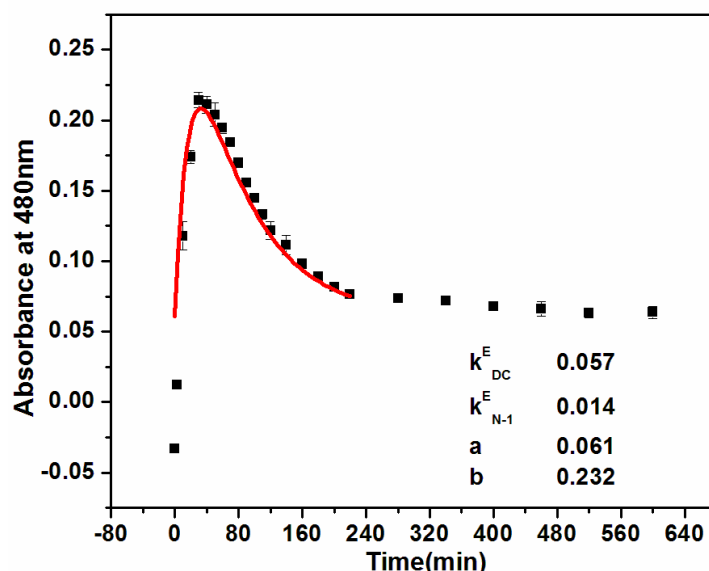
Figure 8.2.3 Absorption kinetics of dopachrome formation and decay kinetics at 480 nm from 0 minute to 600 minutes of the reaction. Fitting parameters are shown (from 0min to 240 min). Abbreviations: k^E_{DC}: Rate of formation of dopachrome, k^E_{N-1}: Rate of formation of the $(N-1)^{th}$ intermediate I_{N-1}, all in the presence of the enzyme, and b: additive and multiplicative constants, all in the presence of the enzyme.

Kinetics of the red intermediate dopachrome which has an absorption band at 480 nm (ε= 3700 M^{-1} cm^{-1})[25] is analyzed by looking at the time-evolution of absorbance at 480 nm as shown in Figure 8.2.3. Meanwhile, kinetics of melanochrome formation is

monitored at 363 nm, since melanochrome has an absorption band at 363 nm as shown in Figure 8.2.2. Melanochrome spectrum was obtained by subtracting the absorption spectrum at 60 minutes (approximately near the time point where dopachrome absorbance is maximum) from the spectrum at 200 minutes, in the presence of the enzyme. This difference spectrum will give us the signature of the intermediate species formed between 60-200 minutes i.e. the species formed after dopachrome formation and the melanin polymer, melanochrome. The absorbance at 363 increases initially while the rate of melanochrome formation is high and slows down due to the formation of the end product melanin, when visible aggregates can be observed in solution. The reduced reaction model for the fits shown in Figures 8.2.2 and 8.2.3 is discussed later.

Plot showing:

$$y = a + k^E_M \cdot t$$

$$a \quad 0.03355$$

$$k^E_M \quad 0.00114$$
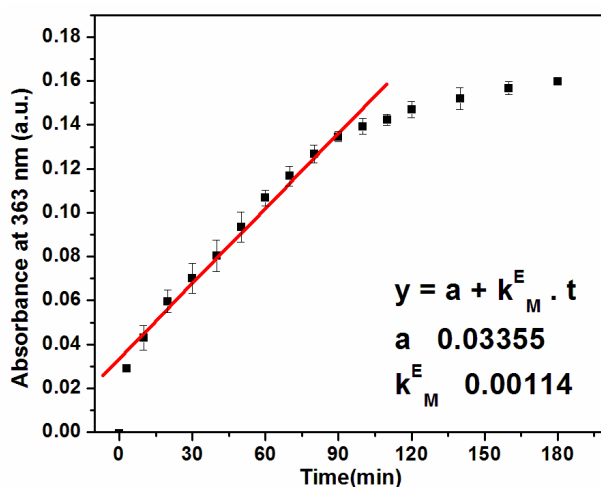
Figure 8.2.4 Absorption kinetics of melanochrome formation at 363 nm from 0 minute to 200 minutes of the reaction. Fitting parameters and equation are shown. Abbreviations: k^E_M: Rate of formation melanochrome in the presence of the enzyme, a: Additive constant.

9   FT- Infra Red spectroscopy of DOPA-melanin formation

Fourier Transform-Infra Red spectroscopy of DOPA-melanin samples (in the absence of enzyme) was performed. The evolution of bands from free DOPA to the auto-oxidized form up to 192 hours is shown in Figure 9.1. The monomer band at 1292cm^{-1}(catecholic C-OH stretch) and the melanin-polymer band at 1616cm^{-1} (aromatic ring stretch) are observed in the FT-IR spectra, as shown in the same figure. As time progresses, we

see the decrease in the intensity of the 1292 cm^{-1} band, and the rise of the 1616 cm^{-1} band.

The broadening of the 1616cm^{-1} band is attributed to the heterogeneity in the polymer population and provides insight into the size distribution of the melanin formed. The broadening of the 1616 cm^{-1} band is observed as asymmetric as opposed to the symmetric broadening seen during the resonance Raman experiment in solution state.
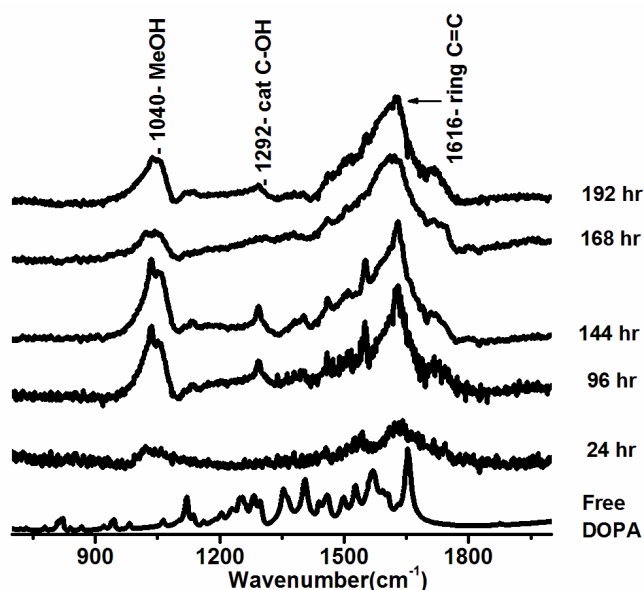
Figure 9.1. FT-IR spectra of auto-oxidized DOPA in the absence of enzyme, in Tris-HCl buffer at pH 7.4 from 0 hours to 192 hours of the reaction. IR bands of interest are marked.

10 Dynamic Light Scattering of DOPA-melanin formation in the absence of enzyme

Dynamic Light Scattering (DLS) measurements were made on the samples at the initial time points of DOPA-melanization and indicated the formation of bigger particles with time. This is as shown in Figure 10.1. The same experiment was carried out by my colleague Sayan Mondal with a larger data set that confirms the growth of particle size over time.
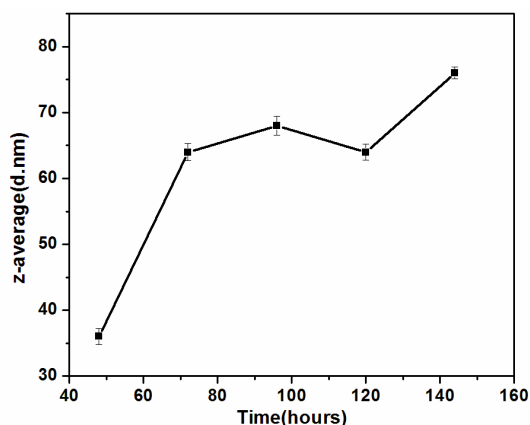
Figure 10.1 DLS z-average data of DOPA-melanin in the absence of enzyme, in Tris- HCl buffer at pH 7.4 from 48 hours to 156 hours of the reaction. Average size of particles increases with time.

11 Resonance Raman spectroscopy kinetics of DOPA-melanin formation

11.1 Resonance Raman kinetics of DOPA-melanin formation in the absence of enzyme (auto-oxidation)

Resonance Raman kinetics of auto-oxidation of DOPA into melanin was monitored at 261 nm in the absence of enzyme tyrosinase up to 199 hours reaction time, in 50 mM Tris- HCl buffer at pH 7.4. The growth of the precursor band at 1292 cm^{-1} vanishes over time, while the polymer peak at 1616 cm^{-1} is seen to become broader with time. The stacked spectrum monitored over time is as shown in Figure 11.1.1.

Kinetics profiles were plotted at two major bands that belong to the precursor DOPA at 1292 cm^{-1} (catecholic C-OH stretch) and that of melanin polymer at 1616 cm^{-1} (aromatic C=C stretch) modes. The kinetics profile of DOPA decay at 1292 cm^{-1} is as shown in Figure 11.1.2 whereas that of melanochrome/melanin at 1616 cm^{-1} is as shown in Figure 11.1.3. The reduced scheme for the fits shown in these figures is discussed later.
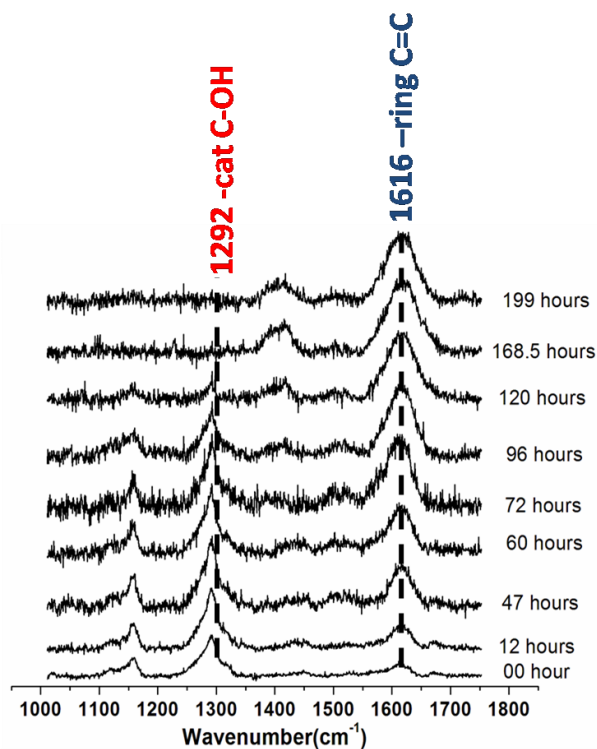
Figure 11.1.1 Raman kinetics at 261nm of DOPA-melanin in the absence of enzyme, in 50 mM Tris-HCl buffer at pH 7.4 from 0 hour to 192 hours of the reaction. The decay of the 1292 cm^{-1} band and rise of 1616 cm^{-1} are shown with their vibrational modes. This experiment has been reproduced from the doctoral thesis of my colleague Sayan Mondal with permission.
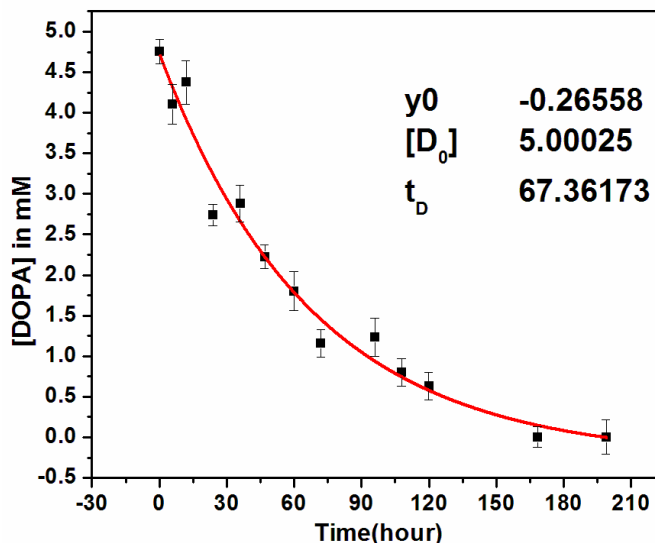
Figure 11.1.2 Raman kinetics of DOPA decay at 1292 cm^{-1} (λ_{exc}=261 nm) from 0 hour to 192 hours of the reaction. Fitting parameters are shown in the figure. Abbreviations: [D$_0$]: Initial concentration of DOPA, t$_D$: time constant for decay of DOPA, y$_0$: additive constant.
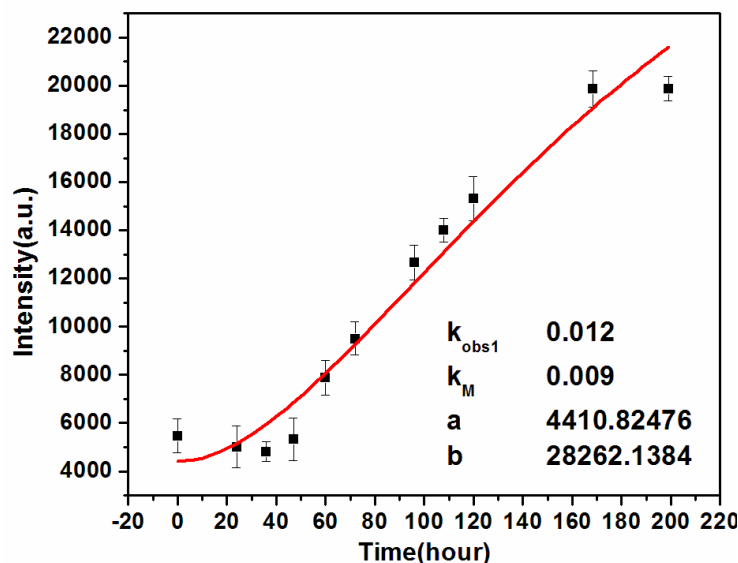
Figure 11.1.3 Raman kinetics of melanochrome formation at 1616 cm^{-1} (λ_{exc}=261 nm) from 0 hour to 192 hours of the reaction. Fitting parameters are shown in the figure. Abbreviations: k$_{obs1}$: Rate of formation of the Nth intermediate I$_N$, k$_M$: Rate of formation of melanochrome, a and b: Additive and multiplicative constants.

11.2 Resonance Raman spectroscopy of DOPA-melanin formation in the presence of enzyme

Resonance Raman kinetics experiment of the enzymatic oxidation of DOPA with tyrosinase was done in 40 mM phosphate buffer up to 700 minutes, at 263 nm. The intensity of 1292 cm^{-1} band of DOPA decreases over time and that of 1616 cm^{-1} band indicating melanochrome formation increases. Furthermore, the latter broadens over time. The 1668 cm^{-1} dopachrome band increases, attains maximum and further decays. The stacked spectra versus time are as shown in Figure 11.2.1.

Kinetics profiles for DOPA decay at 1292 cm^{-1}, melanochrome formation at 1616 cm^{-1} and dopachrome formation and decay at 1668 cm^{-1} (C=O stretching) were monitored with respect to time. The kinetics profiles are as shown in Figures 11.2.2, 11.2.3 and 11.2.5 respectively. The reduced model for the fits as shown in these figures is discussed later.
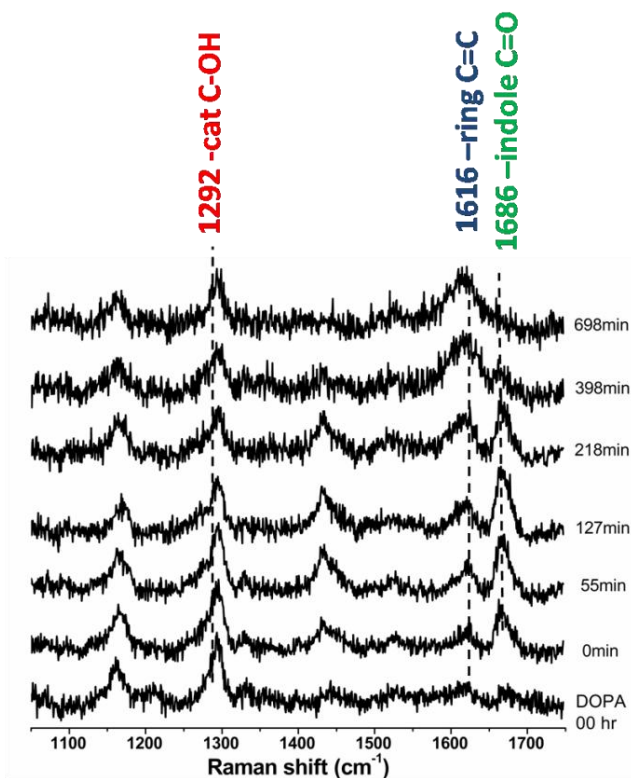
Figure 11.2.1 Raman kinetics at 263 nm of DOPA-melanin in the presence of enzyme, in 40 mM phosphate buffer at pH 6.8 from 0 minute to 698 minutes of the reaction. The decay of 1292 cm^{-1}, the rise of 1616 cm^{-1} and 1668 cm^{-1} are shown with their vibrational modes.
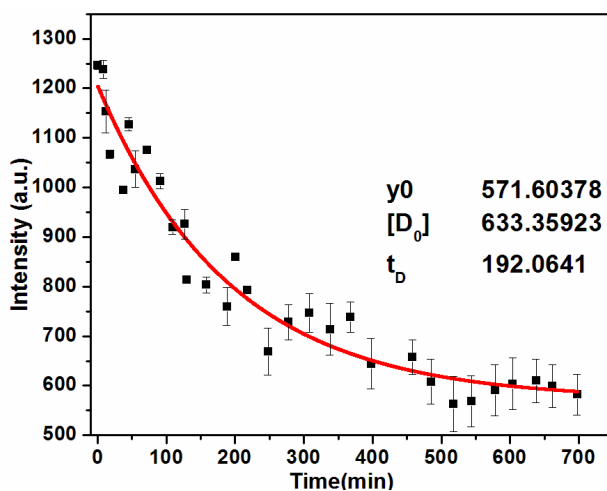
Figure 11.2.2 Raman kinetics of DOPA decay at 1292 cm^{-1} (λ_{exc}=263 nm) from 0 minute to 698 minutes. Fitting parameters are shown. Abbreviations: [D$_0$]: Multiplicative/Normalization constant, t$_D$: Time constant for the rate of decay of DOPA in the presence of the enzyme, y0: additive constant.
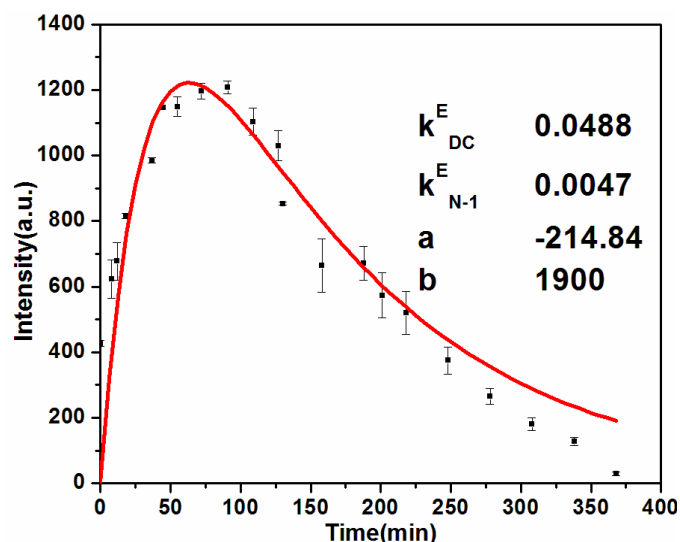
Figure 11.2.3 Raman kinetics of dopachrome formation and decay at 1668 cm^{-1} (λ_{exc}=263 nm) from 0 minute to 400 minutes of the reaction. Fitting parameters are as shown in the figure. Abbreviations: k^E_{DC}: Rate of formation of dopachrome, k^E_{N-1}: Rate of formation of the (N-1)th intermediate, I_{N-1}, a and b: additive and multiplicative constants, all in the presence of the enzyme.

Figure 11.2.4 shows a bi-exponential fit for the decay profile of 1668 cm^{-1} band intensity and Figure 11.2.6 shows the plot of full width at half maximum (FWHM) of the 1616 cm^{-1} band in the presence and absence of the enzyme, both of which are discussed later in the context of interpreting broadening of the marker band of melanochrome formation.
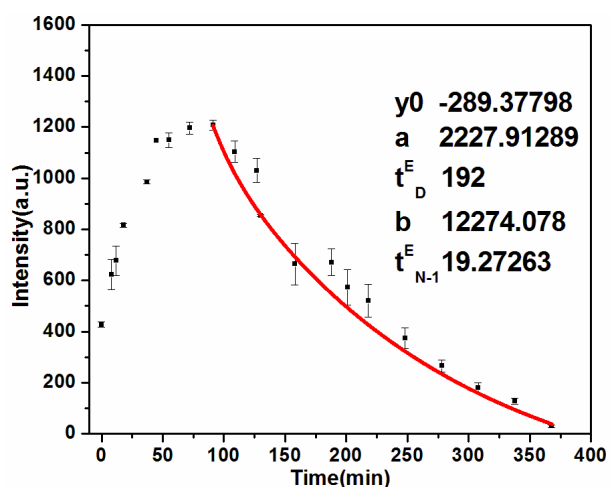
Figure 11.2.4. Raman kinetics of dopachrome at 1668 cm^{-1}(λ_{exc}=263 nm) from 0-400 minutes of the reaction. Bi-exponential decay fitting is done from 90-400 minutes of the decay profile alone. Fitting parameters are shown in figure. Abbreviations: t^E_D: DOPA decay constant, t^E_{N-1}: decay constant of dopachrome, a,b and y0: additive constants

21
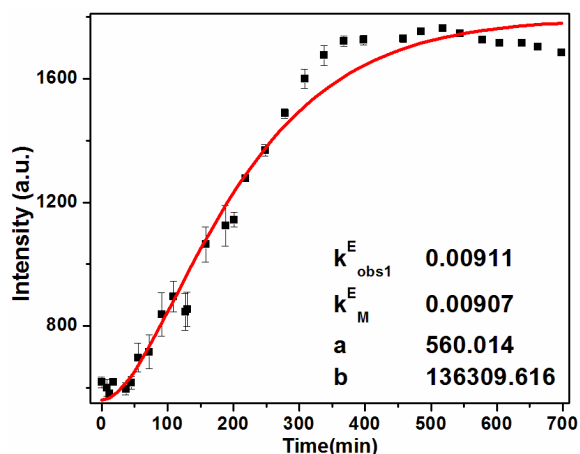
Figure 11.2.5 Raman kinetics of melanochrome formation at 1616 cm^{-1} (λ_{exc}=263 nm) from 0 minute to 698 minutes of the reaction. Fitting parameters are shown in the figure. Abbreviations: k$^{E}_{obs1}$: Rate of formation of the Nth intermediate I$_N$, k$^{E}_{M}$: Rate of formation of melanochrome, a and b: Additive and multiplicative constants, all in the presence of the enzyme.
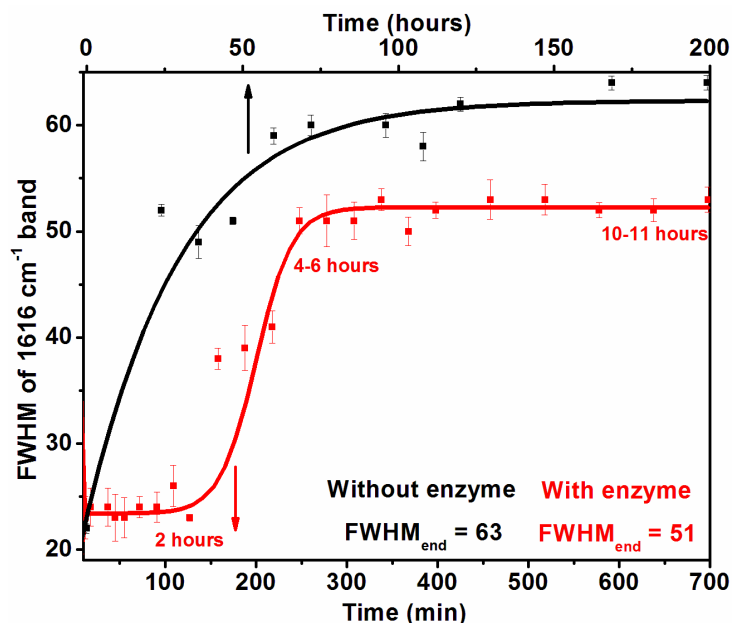
Figure 11.2.6. FWHM of 1616 cm^{-1} band plotted with respect to time, in the presence (red) and absence (black) of the enzyme. Note the difference in timescales shown as two X-axes in the figure. The value of FWHM of the 1616 cm^{-1} band at the end of the experiment is noted as FWHM$_{end}$.

Figure 11.2.7 shows the resonance Raman spectrum of dopachrome recorded at 488 nm. The reduced scheme for the fits shown in the above figures is discussed later, along with the discussion about the rate constants of the reaction.
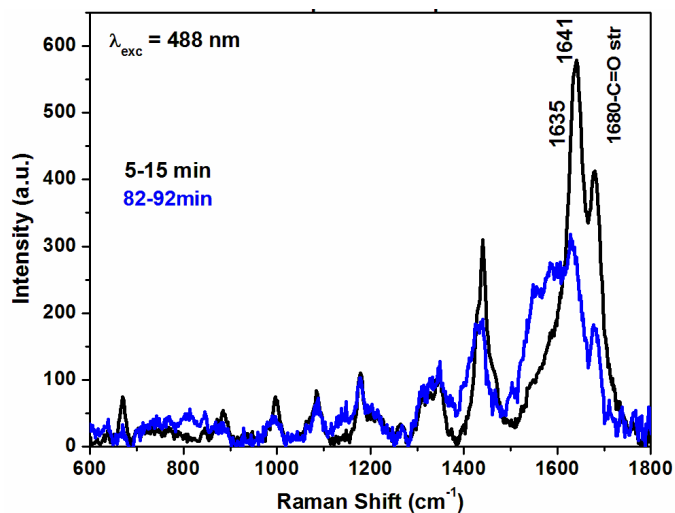
Figure 11.2.7 Resonance Raman spectra of dopachrome at 5-15 min (black) and 82-92 min (blue) of the reaction at 488 nm. Raman bands of interest are marked.

12 Micro-Raman Spectroscopy of various cell types with and without melanosomes at 785 nm

Micro-Raman imaging of melanocytes with treatment of tyrosine and poythiouracil, control cancer cell line HaCaT, primary human keratinocytes and B-16 mouse cells were done at 785 nm. Around twenty hyper spectral images were recorded at optimal imaging conditions per cell type. Figures 12.1.1 and 12.1.2 show the representative set of bright-field images of each cell type and Figure 12.3 shows the corresponding averaged cell Raman signature obtained from area inside the cell at 785 nm. Since cells change their size and shape over various types as seen in Figures 12.1.1 and 12.1.2, the imaging parameters were also different. Band assignments of various components of different cell types observed are as shown in Figure 12.1.3. Primary human melanocytes were scanned along the z-axis value, cutting through the cross-section of the cell at 785 nm. The spectra obtained at different values of z are as shown in Figure 12.1.4.
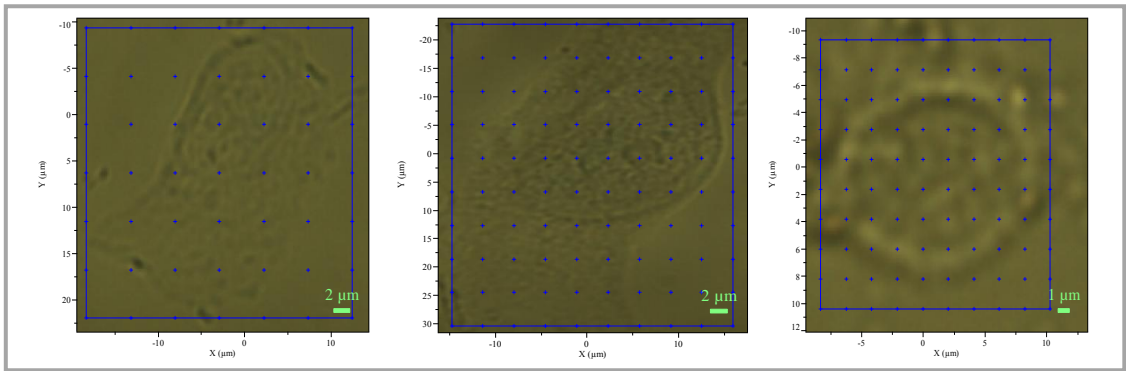
Figure 12.1.1 Bright field images of (a) polythiouracil (PTU) treated primary human melanocytes, (b) tyrosine treated primary human melanocytes and (c) B-16 pigmented mouse cells captured for hyper spectral imaging at 785 nm using Micro-Raman spectroscopy.
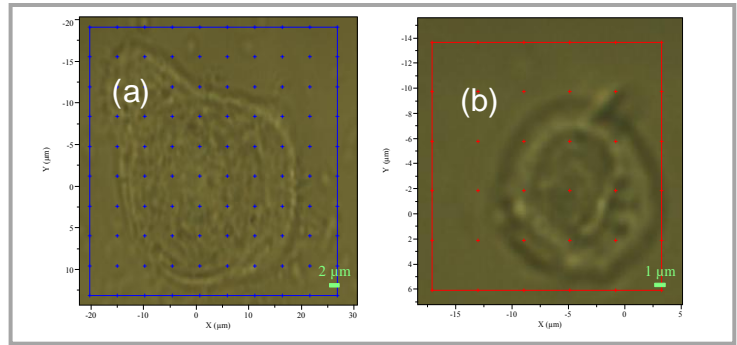
Figure 12.1.2. Bright field images of (a) HaCaT cells (control) and (b) primary human keratinocytes (control) captured for hyper spectral imaging at 785nm using Micro-Raman spectroscopy.
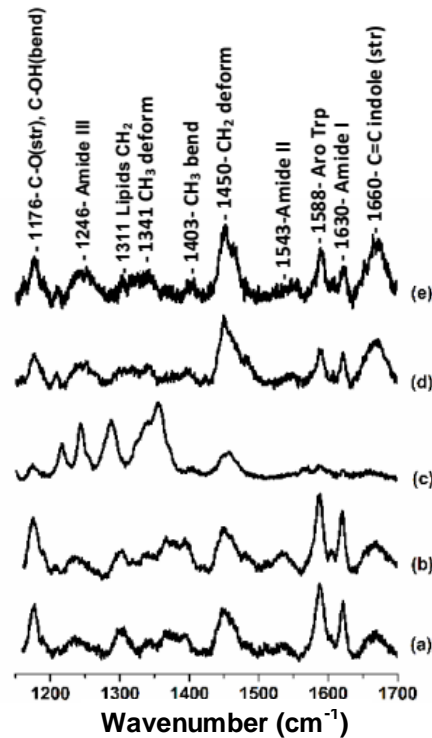
Figure 12.1.3 Averaged Raman spectra from (a) PTU treated primary human melanocyte, (b) tyrosine treated primary human melanocyte, (c) primary human keratinocyte, (d) HaCaT cell and (e) B-16 pigmented mouse cell at 785nm.
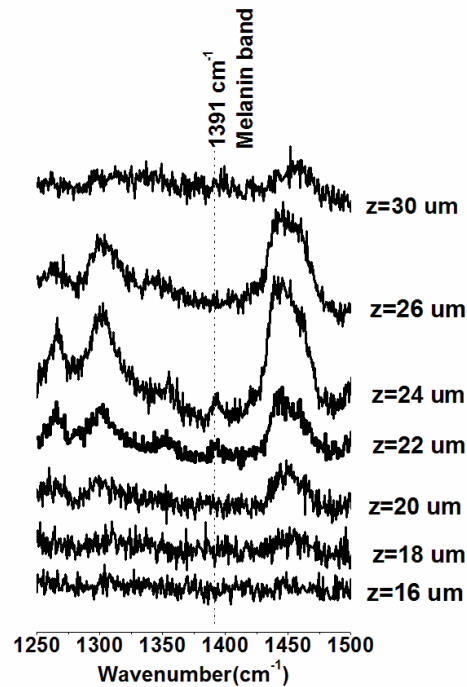
Figure 12.1.4 Vibrational signature of primary human melanocyte captured over a range of z-values from 16µm to 30 µm at 785 nm. The melanin band at 1391 cm^{-1} becomes clearer around z= 24 µm. The melanin band is as marked in the figure.

Discussion

The biggest challenge with the melanin project is the structural and spectroscopic complexity of this biopolymer. The starting point of this work was to understand auto-oxidation of 3,4-dihydrohyphenylalanine (DOPA) i.e. oxidation of DOPA in air atmosphere, denuded of the presence of any chemical regulators or enzymes. In the later part of the work, enzymatic oxidation of DOPA is studied extensively.

13 Auto-oxidation of L-DOPA to melanin polymer

13.1 Reduced model for auto-oxidation of DOPA inspired from Foster's composite reaction model

Absorption spectrum of the reaction (auto-oxidation of DOPA) evolves with time (Figure 8.1.1), which can be directly correlated to the progress of the reaction. Visible blackening of the reaction mixture with time indicates the formation of melanin due to DOPA auto-oxidation. The melanochrome band has been previously reported at 540 nm[26]. However, due to reasons discussed in section 14.1, 540 nm may not be used as marker for melanochrome formation. We see in Figure 8.2.2 that melanochrome has a distinct band at 363 nm as discussed in section 8.2.

Following the work of Foster and others,[27] we have developed a reduced reaction model to explain our experimental observations. Foster's model follows that of a simple composite reaction, as shown in Scheme 1, where A is DOPA, B is dopaquinone and C is melanochrome. In this project, however the intermediates captured differ from that of Foster's model. Hence, while adopting the similar model of that of a composite reaction, the reaction steps that we carefully considered to build the model on is, DOPA to dopachrome to melanochrome to melanin, with certain known/unknown intermediates in between. The modified scheme for auto-oxidation is as shown in Scheme 2.

$$\frac{d[A]}{dt} = -k_1[A]$$

$$\frac{d[B]}{dt} = k_1[A] - k_2[B]$$

$$\frac{d[C]}{dt} = k_2[B]$$

From the above differential equations, we obtain:-

$$[A] = [A]_0 \, e^{-k_1 t}$$

$$[B] = \frac{[A]_0 \, k_1}{k_2 - k_1} [e^{-k_1 t} - e^{-k_2 t}]$$

$$[C] = \frac{[A]_0}{k_2 - k_1} [k_2(1 - e^{-k_1 t}) - k_1(1 - e^{-k_2 t})]$$
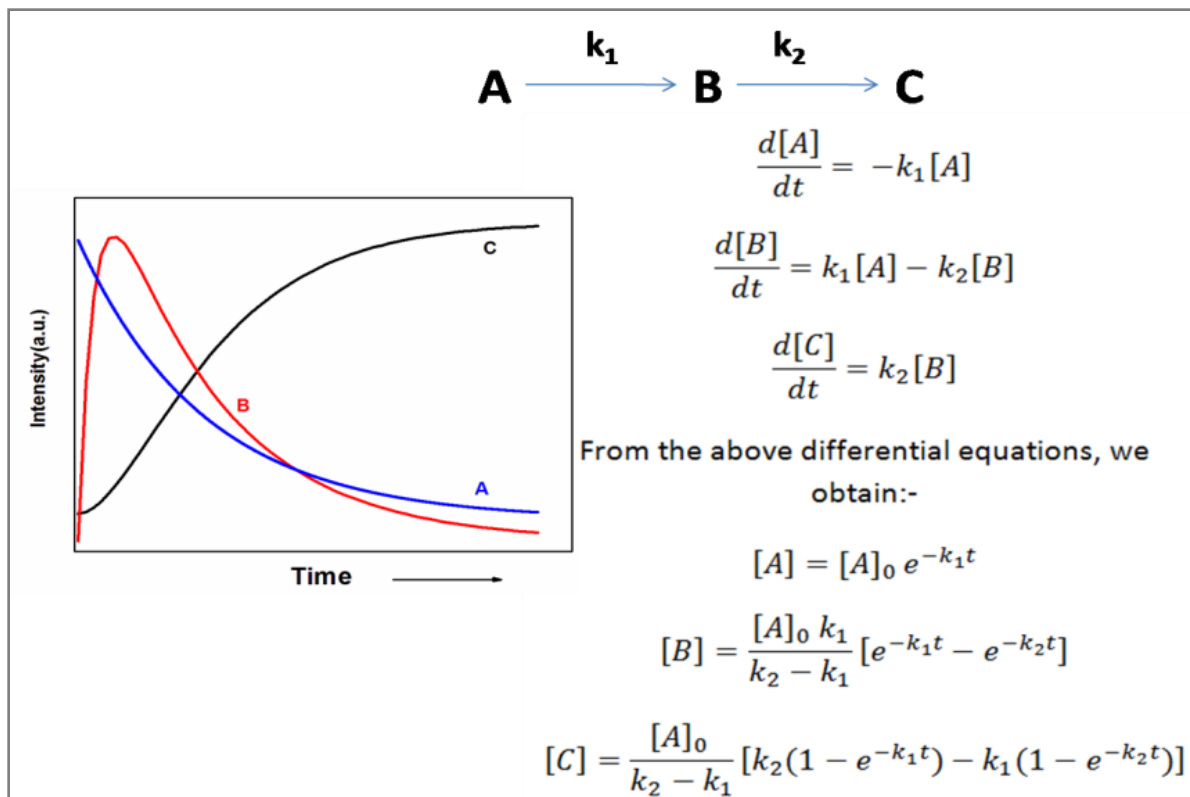
Scheme 4. Foster's model of melanin formation. A is DOPA, B is dopaquinone and C is melanochrome

$$\frac{d[D]}{dt} = -k_D[D]$$

$$\frac{d[DC]}{dt} = -k_{N-1}[DC]$$

$$\frac{d[I_{N-1}]}{dt} = k_{N-1}[DC] \quad k_N \quad bs1[I_{N-1}]$$

$$\frac{d[I_N]}{dt} \quad k_N \quad bs1[I_{N-1}] - k_M[M]$$

$$[D] = y_0 + [D_0]e^{-k_D t}$$

$$\frac{d[M]}{dt} = k_M[I_N]$$

$$[M] = a + \{\frac{b}{k_M - k_N} [k_M(1 - e^{-k_N t}) - k_N(1 - e^{-k_M t})]$$
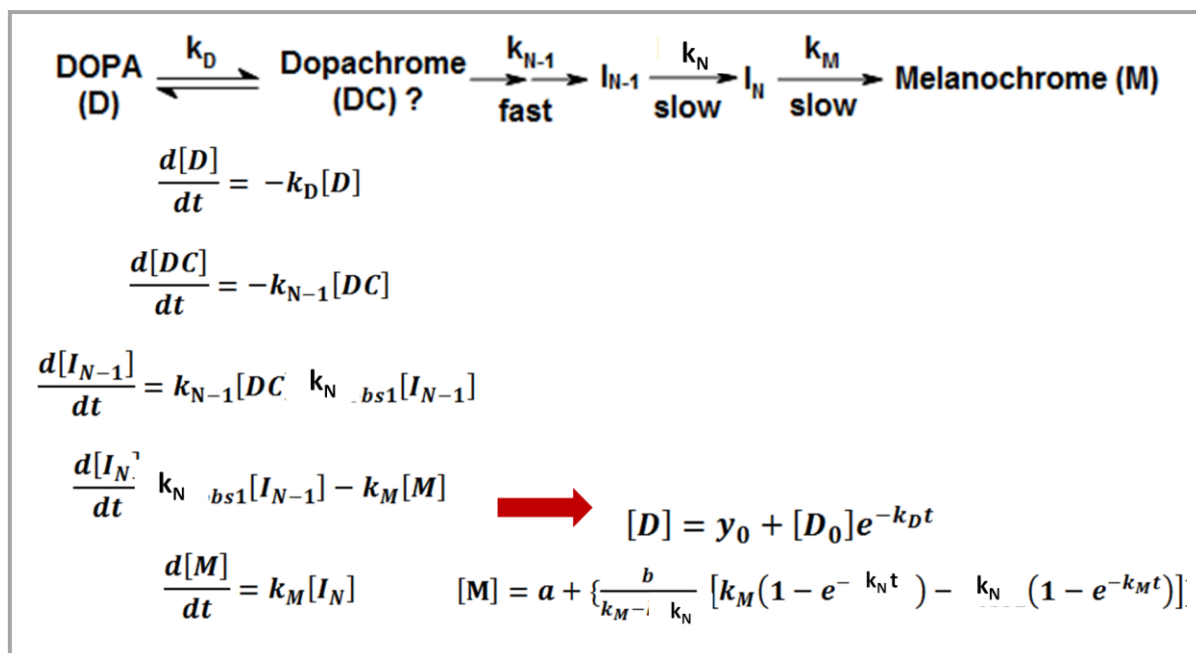
Scheme 5. Reduced model of melanin formation through non-enzymatic oxidation of DOPA. The red arrow indicates the solutions to the differential equations shown.

13.2 Kinetics of DOPA decay from absorption and resonance Raman experiments (auto-oxidation of DOPA)

The DOPA absorption band at 280 nm remains unaltered during the absorption kinetics experiment (Figure 8.1.1). Thus, absorption data cannot tell us about the rate of DOPA getting used up in the reaction or other intermediate rates that are crucial. This suggests that even at the later stages of polymerization and aggregation, the indole skeleton of DOPA remains intact which is responsible for the 280 nm band. Hence, the 280 nm absorption band intensity cannot be used to monitor the decay of DOPA.

The answer to this is to look at the spectroscopic signature of DOPA, along with that of the polymer and any other intermediate species in a single spectrum. This is done naturally in vibrational spectroscopy by which specific vibrational modes of each species in a multiple component reaction are captured. To this effect, FT-IR spectra of auto-oxidized DOPA samples, which confirmed the presence of the catecholic C-OH stretching band at 1292 cm^{-1} of DOPA and the aromatic ring C=C stretching mode of the polymerizing species at 1616 cm^{-1} was obtained in solid state (Figure 9.1). In the FT-IR data, we see that the 1292 cm^{-1} band decreases in intensity over time and that the 1616 cm^{-1} band broadens and grows in intensity over time. The broadening of the 1616 cm^{-1} band is observed as asymmetric as opposed to the symmetric broadening seen in Raman, as discussed below.

In order to study the kinetics conclusively in solution state, the technique of resonance Raman spectroscopy has been used in this project. Since precursor DOPA has an absorption band at 280 nm, when exposed to at 261 nm, its bands will get resonance enhanced. Therefore, resonance Raman kinetics was followed at 261 nm (Figure 11.1.1) and the time evolution of the DOPA band at 1292cm^{-1} and that of the polymer at 1616cm^{-1} are as shown in Figures 11.1.2 and 11.1.3.

Scheme 2 has been used to follow the kinetics of the reaction obtained by Raman spectroscopy as well. The rate of decay of DOPA, k_D is as shown in Scheme 2, an exponential decay. The fitted curve establishes the value of k_D as 2.4×10^{-4} min^{-1}.

13.3 Kinetics of melanochrome formation from absorption and resonance Raman experiments (auto-oxidation of DOPA)

Under the approximation that the rate of decay of dopachrome/rate of formation of the (N-1)th intermediate I_{N-1} (both of which are much faster compared to the timescale of the experiment, due to which go unobserved) $k_{(N-1)}$ (refer to Scheme 2) is much greater than the rate of formation of melanochrome k_M, the kinetics of formation of melanochrome reduces from the equation shown in Scheme 2 to a linear curve governed by the equation,

$$[M] = a + [D_0]\, k_M t\,, \quad \text{when } k_{(N-1)} >> k_M \qquad \textit{Equation 1}$$

where $[D_0]$ is a multiplicative constant. Figure 8.1.2 shows the data fitting with respect to *Equation 1* and thus obtained value of $k_M = 2.3 \times 10^{-5}$ min^{-1}.

But the major difference between the model adopted for absorption data and Raman data arises from the specificity of monitoring a process such as melanochrome formation. The energy resolution of vibrational spectroscopy is of 1000 times more than that of absorption spectroscopy. When a species is looked at through IR/Raman spectroscopy, a specific vibrational mode is captured. Thus kinetic profile at 1616 cm^{-1} reports exclusively about melanochrome and short length polymers having similar ring structure as that of the melanochrome. But this level of specificity is absent in absorption data. Hence, to fit the Raman data kinetics profile at 1616 cm^{-1}, the rate constants under focus should be k_N, the rate of formation of the last intermediate just before melanochrome begins forming and k_M, the rate of formation of melanochrome, unlike in absorption where we looked at the rate of formation of the (N-1)th intermediate k_{N-1} and k_M. Now, under the assumption that $k_N \approx k_M$, the equation for [M] given in Scheme 2 holds.

$$[M] = a + \left\{ \frac{b}{k_M - k_N} \left[k_M \left(1 - e^{-k_N t}\right) - k_N \left(1 - e^{-k_M t}\right) \right] \right\}\,, \quad \text{when } k_N \approx k_M$$

Equation 2

The kinetics profile at 1616 cm^{-1}, as shown in Figure 11.1.3 fitted with equation 2 gives the values of the rate constants as, k_N= 2.0x10^{-4} min^{-1} and k_M= 1.5x10^{-4} min^{-1}.

13.4 Spectral broadening of 1616 cm^{-1} band: Measure of heterogeneity of melanin-polymer population

Another interesting feature of the melanochrome formation kinetics at 1616 cm^{-1} is the phenomenon of spectral broadening with time. Spectral broadening during the course of the reaction is due to the formation of multiple species that have very closely lying vibrational modes in terms of energy. This leads to the theory of formation of heterogeneous population. 5,6-dihydroxyindole (DHI) is one of the monomers that is in the reaction pathway of melanin polymerization. In a theoretical study done by my colleague Sayan Mondal and several other experimental studies,[28] it is shown that polymerization of DHI is most favored at the 2-2, 2-4 and 2-7 positions of the monomers. The possibility of different sites of polymerization leads to heterogeneity in polymerization. This is reflected as the broadening of the 1616 cm^{-1} band. The broadening of this band is seen symmetric in this Raman experiment, as opposed to the asymmetric broadening as seen in FTIR. This maybe because the FT-IR experiment was done in solid state, whiles the Raman experiments were done in solution state, which contributes to the symmetry in broadening. However, IR data is anticipated to give a better view at the different types of polymers that are being formed from the light of the current study.

14 Absorption kinetics of enzymatic oxidation of DOPA to melanin polymer

14.1 Dopachrome stabilization and the presence of other intermediates

To investigate the role of the enzyme tyrosinase in melanogenesis, melanin formation kinetics by oxidation of DOPA in the presence of the enzyme was looked at in the second part of this study. While the enzyme reaction takes place faster than the non-enzymatic auto-oxidation of DOPA, we see the formation and stabilization of a red-

colored intermediate during the course of the reaction (as discussed in section 15.1). We were able to capture this red-intermediate for long enough to look at its kinetics since the reaction was carried out in purged (with Argon) conditions, thus making oxygen a limiting factor in the reaction.

The absorption curves show distinct marker bands for dopachrome as a low intensity band at 250 nm, an intense 305 nm band and a broad band (≈100 nm FWHM) at 480 nm (Figure 8.2.2). It is likely that on the event of dopachrome formation during the course of the reaction, the 480 nm band will contribute to the absorbance at 540 nm. Thus contrary to previous reports[17], 540 nm cannot be used as a marker band for monitoring the formation of melanochrome. The melanochrome band at 363 nm is well resolved if we look at the difference spectra between a spectrum at the near-end of the reaction (600 minutes) and at an earlier time point such as 60 minutes, as shown in Figure 8.2.2. Thus for the first time, we report kinetics of melanochrome formation at 363 nm.

An important feature seen in the absorption kinetics profile is evidence for formation of longer melanin polymer-products. We see that the dopachrome peak at 480 nm red-shits with time to as far as 570 nm which is a broader peak. This is because the populations of dopachrome present at the initial stages of the reaction forms other intermediates which are untraceable in the present study, forms various polymer units of melanin. In the biosynthetic pathway of melanogenesis dopachrome is converted into DHI or DHICA under certain conditions. In the scope of the current study, only DHI units are formed from dopachrome since the formation of DHICA calls for the presence of the enzyme Trp2 or dopachrome tautomerase.[29] As DHI units are formed, they start polymerizing which results in extending the ring conjugation that leads to decreasing the HOMO-LUMO gap which causes this red-shift. Upon subtraction of spectra of the 20 minutes spectrum from the 30 minutes spectrum onwards, a narrow distinct peak at 298 nm is also seen which has been reported to be the DHI peak.[30] However, the rate constants obtained by the kinetics profile at 298 nm will not give the absolute rate constants since the absorbance at 298 nm has substantial contribution from the adjacent 280 nm and 305 nm peaks which have much higher molar absorptivity

31

constants. Once melanin polymers have formed, they contribute to the visible region of the absorption spectrum. Hence, the kinetics information that we get from the profiles at 363 nm (melanochrome formation) and 480 nm (dopachrome kinetics) will be over-estimated. However, the kinetics data before the interference from the polymers initiate at the initial time points still give us insight about ongoing processes.

14.2 Kinetics of dopachrome and melanochrome: Reduced model of melanin polymerization

$$\text{DOPA (D)} \underset{}{\overset{k_D}{\rightleftharpoons}} \text{Dopaquinone (DQ) ?} \xrightarrow[\text{fast}]{k^E_{DC}} \text{Dopachrome (DC)} \xrightarrow[\text{fast}]{} \rightarrow \text{DHI} \longrightarrow$$

$$\frac{d[D]}{dt} = -k^E{}_D[D]$$

$$\xrightarrow{k^E_{N-1}} I_{N-1} \xrightarrow[\text{slow}]{k^E_N} I_N \xrightarrow[\text{slow}]{k^E_M} \text{Melanochrome (M)}$$

$$\frac{d[DC]}{dt} = k^E_{DC}[D] - k^E{}_{N-1}[DC]$$

$$\frac{d[I_{N-1}]}{dt} = k^E{}_{N-1}[DC] - k^E{}_N [I_{N-1}]$$

$$\frac{d[I_N]}{dt} = k^E{}_N [I_{N-1}] - k^E{}_M[I_N]$$

$$\frac{d[M]}{dt} = k^E{}_M[I_N]$$

$$[D] = y_0 + [D_0]e^{-k^E{}_D t}$$

$$[DC] = a + \left\{ b. \frac{k^E_{DC}}{k^E{}_{N-1} - k^E{}_{DC}} \left(e^{-k^E{}_{DC}t} - e^{-k^E{}_{N-1}t} \right) \right\}$$

$$[M] = a + \left\{ \frac{b}{k_M - k_N} \left[k_M(1 - e^{-j k_N t}) - k_N (1 - e^{-k_M t}) \right] \right\}$$
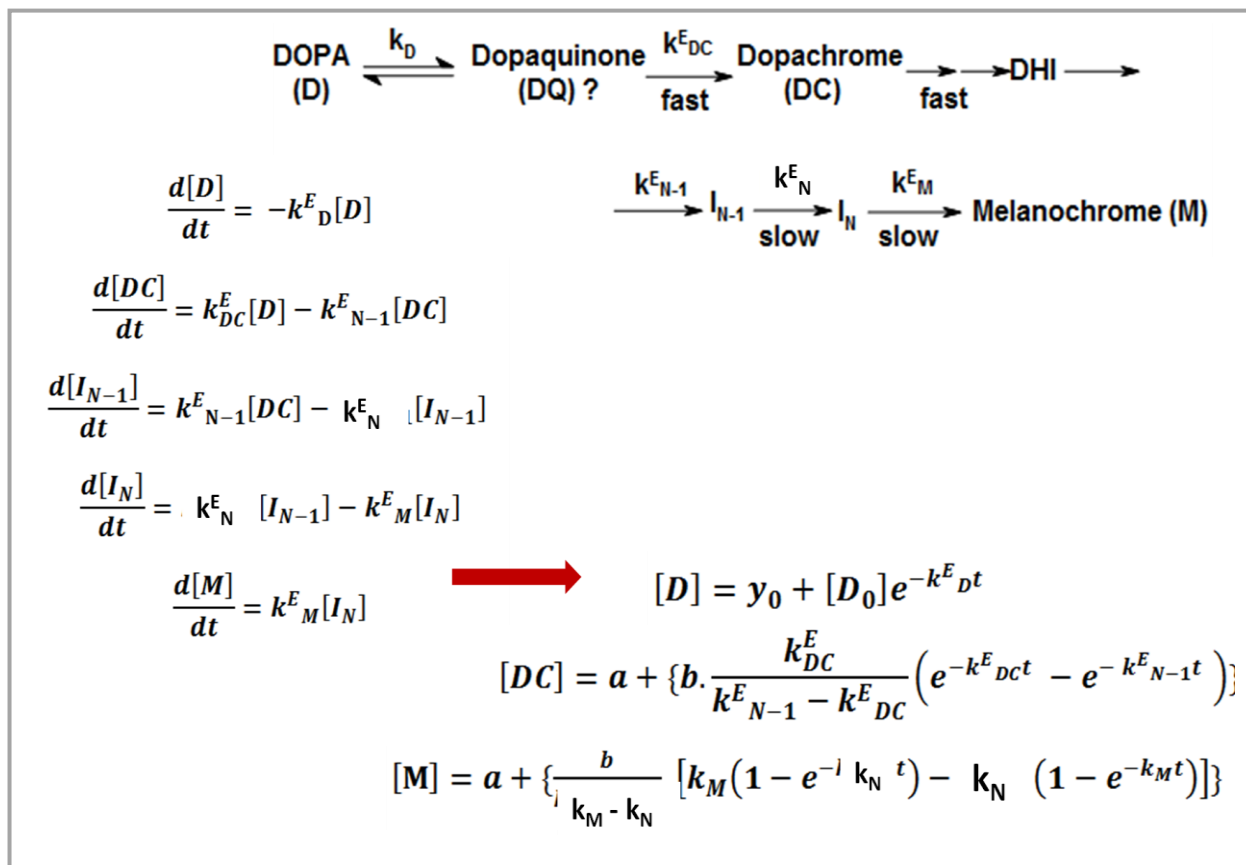
Scheme 6. Reduced model of melanin formation through enzymatic oxidation of DOPA. The red arrows indicate the solutions to the differential equations shown.

To rationalize the kinetics data obtained from the absorption experiment, a new reduced model different from that shown in Scheme 2 was developed. Scheme 2 cannot be applied on the kinetics data with enzyme since there are new intermediates that have been stabilized by the enzyme. The new reduced model is as shown in Scheme 3.

Since DHI is a highly unstable species and the rates associated with it are immensely high, the rate of formation of the $(N-1)^{th}$ intermediate, $k^E_{(N-1)}$ can be treated as equivalent to the rate of decay of dopachrome. Hence, $k^E_{(N-1)}$ is treated as the rate of decay of dopachrome. Under the approximation that the rate of dopachrome decay ($k^E_{(N-1)}$) is much greater than the rate of melanochrome formation (k^E_M), the kinetics of formation of melanochrome reduces to a linear equation as given below. The kinetics of dopachrome formation and decay will be given by Equation 4 (also shown in Scheme 3).

$$[M] = a + [D_0]\, k^E_M t\,, \quad \text{when } k^E_{(N-1)} >> k^E_M \qquad \textit{Equation 3}$$

$$[DC] = a + \left\{ b.\frac{k^E_{DC}}{k^E_{(N-1)} - k^E_{DC}} \left(e^{-k^E_{DC}t} - e^{-k^E_{(N-1)}t} \right) \right\} \quad \textit{Equation 4}$$

The kinetics profile of absorbance data at 480 nm (Figure 8.2.3) is fit to *Equation 4*, which gives the value of the rate of formation of dopachrome, $k^E_{DC} = 5.7 \times 10^{-2}$ min^{-1} and the rate of decay of dopachrome, $k^E_{(N-1)} = 1.4 \times 10^{-2}$ min^{-1}. The kinetics profile of absorbance data at 363 nm (Figure 8.2.4) is fit to Equation 3, which gives the rate of formation of melanochrome, $k^E_M = 1.14 \times 10^{-3}$ min^{-1}.

14.3 Significance of isosbetic points in the time-dependent absorption data of melanin polymerization

A very interesting aspect of the absorption kinetics data is the presence of two isosbetic points at 403 nm and 339 nm seen between 20 minutes and 340 minutes of the reaction as seen in Figure 8.2.1. Isosbetic point is defined by IUPAC as the "wavelength, wavenumber or frequency at which the total absorbance of a sample does not change during a chemical reaction or a physical change in the sample".[31] Earlier, the presence of isosbetic points in an ongoing reaction mixture was misinterpreted to be the proof of conversion of one species to another unique species or the presence of equilibrium between only two species. However, the observation of a single isosbetic point proves the presence of only two absorbing species when one reacting species gets converted to another; at the wavelength at which both absorption species overlap gives the isosbetic point.[32] More recent research has further shown that the presence of isosbetic

point concludes that the stoichiometry of the reaction remains unchanged during its course. In 2008, A. E. Croce[32] proposed mathematically that the presence of one or more isosbetic points suggest that the observed process is a parallel reaction and also that, in a consecutive reaction, isosbetic point(s) will not be observed. The reaction kinetics profiles of DOPA, dopachrome and melanochrome as we observe and previously established,[4] follows a composite/consecutive reaction mechanism. Some intermediates like DHI are identified as the previously reported[3] 298 nm narrow band in the difference absorbance spectra, and weak Raman bands at 1165 cm^{-1}(combined C-H in plane and O-H mode) and 1336 cm^{-1} (ring deformation in pyrrole combined with benzene breathing mode)[33] in the Raman experiment at 263 nm, but cannot be studied kinetically since these bands are poorly defined in the time-evolution spectra. Since the intermediates proposed during the course of melanogenesis can only be detected but not studied in detail due to their short lifespan, in the light of the work by Croce's work we can conclude that though we are following a complicated consecutive reaction, where some steps like the conversion of DOPA to dopachrome to DHI may seem like a parallel reaction i.e. conversion of DOPA to dopachrome and DHI happen simultaneously. This validates that the kinetics of "unseen" intermediates in melanogenesis is very fast.

15 Resonance Raman kinetics of enzymatic oxidation of DOPA to melanin polymer

Following the time dependent absorption experiment to monitor enzymatic oxidation of DOPA with tyrosinase, time dependent resonance Raman experiment on the enzymatic oxidation of DOPA was also carried out at λ_{exc}= 263 nm. The results are as categorized below.

15.1 Stabilization of dopachrome by tyrosinase and other aspects of enzymatic oxidation of DOPA

Like we saw from the time dependent absorption spectra of the enzymatic oxidation of DOPA, dopachrome getting stabilized is also captured through the resonance Raman

experiment. But unlike the absorption data, due to the specificity of probing a particular mode of vibration through Raman spectroscopy, the kinetics data from Raman experiment is more reliable. The Raman band at 1292 cm^{-1} belongs to the catecholic C-OH stretching mode of the precursor, DOPA as discussed before in the non-enzymatic case, and hence it is employed to look at the rate of decay of DOPA during the entire course of the reaction. The dopachrome vibrational mode that has been used to make its kinetics profile is 1668 cm^{-1}, which is the C=O mode on the indole ring. The intensity of the 1668 cm^{-1} band increases in the beginning, with a steep slope till 70-80 minutes, and starts falling in an exponential manner, as shown in Figure 11.2.4. The absorption data kinetics at 480 nm also tells us a similar story. As discussed before, the band at 1616 cm^{-1} is assigned to the aromatic C=C stretching mode of the benzene ring. Thus, the extent of polymerization or the formation of melanochrome is gauged by the intensity of the 1616 cm^{-1} band. We can clearly see from Figure 11.2.4 that the intensity of the 1616 cm^{-1} band increases (overcoming the initial lag phase) and saturates over time.

15.2 Kinetics of DOPA, dopachrome and melanochrome using resonance Raman: Enzymatic oxidation of DOPA

The reduced model adopted for the enzymatic oxidation of DOPA shown in Scheme 3 is utilized here as well. The decay kinetics of DOPA studied at 1292 cm^{-1} is followed by *Equation 5* and the kinetics of dopachrome studied at 1668 cm^{-1} is given by *Equation 4*. Unlike in absorption, the assumption of $k^E_{(N-1)} \gg k_M$ leading to *Equation 4* for the kinetics of melanochrome formation cannot be used in the Raman data. The similar case discussion taken up for drawing the difference in the assumptions between the interpretation of absorption and Raman kinetics data in the non-enzymatic case should be followed here as well. Thus, the kinetics profile of the Raman band at 1616 cm^{-1} will tell us only about melanochrome kinetics and the kinetics of the species most closely related to that of melanochrome, which is the Nth intermediate, I_N. Hence, the equation for melanochrome (M) will be governed by the rate of formation of I_N, k^E_N and the rate of formation of melanochrome, k^E_M, which is given by *Equation 6*, below.

$$[D] = y_0 + [D_0]e^{-k^E_D t} \qquad \text{Equation 5}$$

$$[M] = a + \left\{ \frac{b}{k^E_M - k^E_N} \left[k^E_M \left(1 - e^{-k^E_N t}\right) - k^E_N \left(1 - e^{-k^E_M t}\right) \right] \right\}, \qquad \text{when } k^E_N \approx k^E_M$$

$$\text{Equation 6}$$

The fit of *Equation 5* of DOPA decay kinetics is as shown in Figure 11.2.1 and fitted value of the rate of DOPA decay k^E_D is 5.2×10^{-3} min^{-1}, while that in the absence of the enzyme is $k_D = 2.4 \times 10^{-4}$ min^{-1}. This leads to the conclusion that DOPA decay is faster here because product is being removed from the reaction by tyrosinase.

Equation 4 gives the rate of formation of dopachrome, $k^E_{DC} = 4.88 \times 10^{-2}$ min^{-1} and the apparent rate of decay of dopachrome, $k^E_{(N-1)} = 4.7 \times 10^{-3}$ min^{-1} from the Raman kinetics profile at 1668 cm^{-1}. The absorption kinetics at 480 nm gives a similar value of k^E_{DC} (5.7×10^{-2} min^{-1}) independently, whereas the decay rate of dopachrome is higher from absorption data fitting (1.4×10^{-2} min^{-1}) than observed from the Raman data (4.7×10^{-3} min^{-1}). This cannot be rationalized since the rate of overall decay of dopachrome and related species should be lower in the absorption kinetics at 480 nm since melanochrome formation overshadows the pure dopachrome decay, as opposed to the Raman data which shows dopachrome and only very closely related species decay.

Free DOPA when comes in contact with O_2 in solution gets oxidized, and thus formed carbonyl group on the indole ring gives rise to the observed band at 1668 cm^{-1}. The kinetics profile at 1668 cm^{-1} monitors the carbonyl group on the indole ring, which is thus common to both dopachrome and DOPA. Hence, while monitoring the decay of the carbonyl band, we should consider a bi-exponential decay which consists of both DOPA decay as well as dopachrome decay. Thus, the kinetics profile at 1668 cm^{-1} (only the decay region) was fitted with a bi-exponential decay curve as given in *Equation 7* from 90-400 minutes (shown in Figure 11.2.4), apart from fitting it with *Equation 4* in the whole range of 0-400 minutes (shown in Figure 11.2.2).

$$[DC]_{decay} = y_0 + a.e^{\left[\frac{-t}{t^E_D}\right]} + b.e^{\left[\frac{-t}{t^E_{(N-1)}}\right]}, \qquad \text{Equation 7}$$

where t^E_D is the rate constant of DOPA decay and t^E_{N-1} is the rate constant of dopachrome decay given by,

$$\mathbf{t^E_D = \frac{1}{k^E_D}} \quad \text{and} \quad \mathbf{t^E_{(N-1)} = \frac{1}{k^E_{(N-1)}}} \qquad \textit{Equation 8}$$

In the bi-exponential decay curve following *Equation 7*, one of the rate constants was fixed as the DOPA decay rate from 1292 cm^{-1} decay (k^E_D= 5.2x10^{-3} min^{-1}) , while other parameters were varied. The bi-exponential fit gave us the pure dopachrome decay constant, $k^E_{(N-1)}$ = 5.18x10^{-2} min^{-1}. Now, this pure decay rate of dopachrome is much higher than the apparent dopachrome decay rate obtained from absorption at 480 nm. Thus, the decay of dopachrome formation follows bi-exponential behavior. Also, the rate of formation of dopachrome (k^E_{DC}= 4.88x10^{-2} min^{-1}) and that of pure decay of dopachrome ($k^E_{(N-1)}$= 5.18x10^{-2} min^{-1}) are very similar. This should ideally be reflected with a symmetric kinetics profile at 1668 cm^{-1}, however this symmetry is lost since the apparent/observed decay of the 1668 cm^{-1} band has contributions from both DOPA and dopachrome decay. This however does not affect the initial rise of the intensity of the 1668 cm^{-1} band since it is at lower intensity values of this band that the rate constant of DOPA decay, k^E_D (which is a 10 times smaller number when compared to the rate of formation of dopachrome) creeps in.

15.3 Regulation of the heterogeneity of melanin polymer by tyrosinase

The FWHM plots of 1616 cm^{-1} band with and without enzyme are shown in Figure 11.2.6. While there is a distinct lag phase in broadening of the 1616 cm^{-1} band in the presence of the enzyme tyrosinase, there is an immediate exponential (growth) phase when tyrosinase is absent. But clearly the growth phase is steeper when tyrosinase is present, which shows that there is an obvious threshold of a parameter (which could be concentration of an intermediate, or any another reaction co-ordinate which is beyond the scope of the present study), only after which melanochrome reaches its saturation phase. In the presence of the enzyme, the curve saturates at a much lesser FWHM value (FWHM$_{end}$: 51 cm^{-1}) than in the absence of the enzyme (FWHM$_{end}$: 63 cm^{-1}). This implies that the heterogeneity of population is much lower in the presence of the

enzyme than in the non-enzymatic case. From these observations it is reasonable to conclude that the enzyme imposes a regulation in the formation and heterogeneity of the melanin polymer. It can also be inferred that distribution of the no: of types (depending on the site of polymerization, as discussed in section 13.4) of melanin polymers is narrow when the enzyme is present. The sharp threshold between the lag phase and the saturation phase, and the extent of saturation ($FWHM_{end}$) are features that define this regulatory action of tyrosinase. However, since the average frequency of the ring mode 1616 cm^{-1} is the same in the presence and absence of tyrosinase, we may also conclude that melanin polymers formed by auto-oxidation and in the presence of tyrosinase are similar in monomer units formed, although the heterogeneity at the polymer-level varies significantly.

16 Micro-Raman vibrational spectroscopy of melanocytes versus non-melanocytes

Vibrational spectroscopy coupled with imaging using microscopy was performed in order to understand the spatial distribution of various cell components, though the primary aim was to locate melanosomes. However, since the concentration of other cellular components like lipids, proteins, nucleic acids etc are much higher than that of melanin or melanosomes, signals from melanin was not successfully obtained. However, average cellular spectra (after background correction) for all five different types of cell types are as shown in Figure 12.1.3 and the corresponding bright field images are shown in Figures 12.1.1 and 12.1.2.

Treatment of melanocytes with polythiouracil (PTU) is reported to inhibit the production of melanin inside cells, while supplying cells with the melanogenetic precursor tyrosine is known to increase the production of melanin. However, in the current study, hardly any spectral dissimilarity was seen between the two. The common elements in the spectra of PTU and tyrosine treated cells, HaCaT cells which are the cancer line of keratinocytes and B-16 mouse pigmented cells is many like, 1176 C-O stretch and C-OH bend, broad 1246 amide III band, 1403 CH$_3$ bend, 1450 CH$_2$ deformation, 1543

amide II, 1630 amide I and the broad C=C indole stretching mode, which are previously reported.[22,23] Though all these are common vibrational modes present, the relative intensity of the peaks vary with the cell type. The most distinct spectrum is of primary human keratinocytes (PHK). While Amide II mode is mostly broad for all other cell types, in PHK it is very narrow and well defined. Also, the intensity of lipid modes like CH_3 bend (1403) and CH_2 deformation (1450) is much more intense in PHK when compared to others.[21]

16.1 Spotting melanosomes in melanocytes

Melanosomes, the organelles were melanin is synthesized, stored and transported to other cellular sites are located along the periphery of cells. Since the concentration of melanosomes (and thus, melanin) is minor compared to that of other cellular components such as lipids, proteins and the like, the melanin signature has to be looked for in another way. For imaging of cells that are not alive, cells are mounted on a flat quartz slide and fixed the way mentioned in the experimental section. These cells which are fixed on the slides are however not flat, rather looking like a part of a hemisphere which tends to being flat along the edges. Hence, we realized that a z-value map i.e. scanning the probe laser (785 nm) through the cross section of the cell will lead us to the cross-sectional area of the cell where melanosome concentration is the maximum. Melanin band has been elsewhere reported around 1380 cm^{-1}, for *in vivo* melanin of human skin.[24] From Figure 12.1.4, we see that from z= 16 μm to z=20 μm, the melanin band is not observed. But from z=20 μm to z= 26 μm, we see a systematic change in the intensity of the 1391 cm^{-1} melanin band, which peaks at z= 24 μm. Beyong z= 26 μm, the 1391 cm^{-1} band vanishes. Note that other band intensities are also varying with respect to the change in the z-value. Hence, we conclude that inorder to specifically look for melanin in a quantitative manner, the cross-sectional scanning of cells has to be performed.

Conclusions

The current study's focus has been to look at the kinetics of two reactions that lead to the formation of melanin polymer: auto-oxidation of DOPA and enzymatic oxidation of DOPA. Reduced models of both of the above mentioned composite reactions were developed and rates of the intermediates were analytically established. The entire reaction scheme with rate constants are as shown in Figure 13.1 and all the rates characterized in the current study are tabulated in Table 1. The rates of various intermediates in the presence and absence of the enzyme show that enzymatic oxidation of DOPA occurs at least ten times faster than auto-oxidation of DOPA. DOPA decay is observed to occur faster in the presence of the enzyme, and it is postulated in this work that this happens because the enzyme stabilizes the product being formed in that step. An intermediate, dopachrome was found to be stabilized by the enzyme as well. A major revelation from the current study is the regulatory action of tyrosinase of the heterogeneity of the melanin polymer being formed. The extended lag phase in the broadening of the kinetics profile of melanochrome formation at 1616 cm^{-1}, along with a lower final FWHM of the band observed justifies this heterogeneity regulation by the enzyme. However, since the average peak value remains unaltered at 1616 cm^{-1}, the nature of the monomeric units in both cases are the same. Heterogeneity or the distribution of different types of melanin polymers that are formed can be studied better with FT-IR spectroscopy than Raman spectroscopy. This is because in IR spectrum, the 1616 cm^{-1} band broadens asymmetrically while that in Raman assumes symmetric broadening. While an explanation has to be still obtained, FT-IR spectroscopy can thus bring out more information about the heterogeneity of the melanin-polymer population. The kinetics of various intermediates was not studied in the current study since the reaction rates were too high to be detected. This is a limitation of this project.

Micro-Raman spectroscopic studies of cells containing melanin showed a very crucial result. While the melanin signature is over-shadowed by other cell components present in abundance, a z-value scan through the cross-section of the cell reveals clear Raman

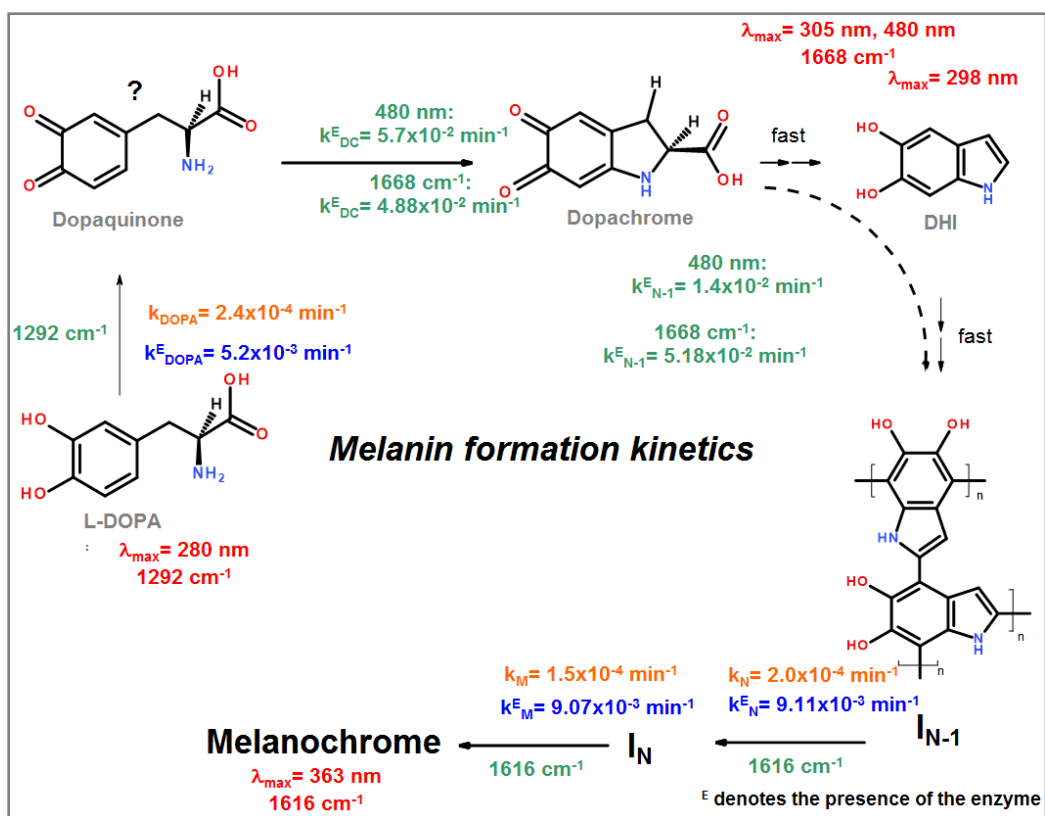signature of melanin from where melanocytes are localized in a particular limit of cross-section of the cell.

Figure 13.1 Reaction scheme of melanin formation. All rate constants found in this study has been represented here, in entirety.

	Raman Intensity (a.u.)			Absorbance (a.u.)	
	$1292\ cm^{-1}$	$1616\ cm^{-1}$	$1668\ cm^{-1}$	480 nm	363 nm
$k_D\ (min^{-1})$	2.4×10^{-4}				
$k_N\ (min^{-1})$		2.0×10^{-4}			
$k_M\ (min^{-1})$		1.5×10^{-4}			2.3×10^{-5}
$k^E_D\ (min^{-1})$	5.2×10^{-3}				
$k^E_{DC}\ (min^{-1})$			4.88×10^{-2}	5.7×10^{-2}	
$k^E_{N-1}\ (min^{-1})$			5.18×10^{-2}	1.4×10^{-2}	
$k^E_N\ (min^{-1})$		9.11×10^{-3}			
$k^E_M\ (min^{-1})$		9.07×10^{-3}			1.14×10^{-3}

Table 2. Rate constants calculated in this study, with and without enzyme. [E] denotes the presence of enzyme.

References

1. Duff, G. a, Roberts, J. E. & Foster, N. Analysis of the structure of synthetic and natural melanins by solid-phase NMR. *Biochemistry* **27,** 7112–7116 (1988).

2. Land J, Edward, Rasden A, Christopher and Riley A, P. in *Methods Enzymol.* **378,** 88–109 (2004).

3. Henry, B. Y. & Raper, S. The tyrosine-tyrosinase reaction. VI Production from tyrosine of 5:6-dihydroxyindole and 5:6-dihydroxyindole-2-carboxylic acid- the precursors of melanin. *Biochem. J.* **21,** 89–96 (1926).

4. Mason, S. The Chemistry of Melanin III. Mechanism of oxidation of dihydroxyphenylalanine by tyrosinase. *J. Biol. Chem.* 83–99 (1947).

5. Moses, H. L., Ganote, C. E., Beaver, D. L. & Schuffman, S. S. Light and electron microscopic studies of pigment in human and rhesus monkey substantia nigra and locus coeruleus. *Anat. Rec.* **155,** 167–183 (1966).

6. Simon, J. D., Hong, L. & Peles, D. N. Insights into Melanosomes and Melanin from Some Interesting Spatial and Temporal Properties. *J. Phys. Chem. B* **112,** 13201–13217 (2008).

7. Ju, K., Lee, Y., Lee, S., Park, S. B. & Lee, J. Bioinspired Polymerization of Dopamine to Generate Melanin-Like Nanoparticles Having an Excellent Free-Radical-Scavenging Property. *Biomacromolecules* **12,** 625–632 (2011).

8. Seagle, B.-L. L., Gasyna, E. M., Mieler, W. F. & Norris, J. R. Photoprotection of human retinal pigment epithelium cells against blue light-induced apoptosis by melanin free radicals from Sepia officinalis. *Proc. Natl. Acad. Sci. U. S. A.* **103,** 16644–16648 (2006).

9. Boulton, M., Rozanowska, M. & Rozanowski, B. Retinal photodamage. *J. Photochem. Photobiol. B Biol.* **64,** 144–161 (2001).

10. Jimbow, K., Quevedo, W. C., Fitzpatrick, T. B. & Szabo, G. Some aspects of melanin biology: 1950-1975. *J. Invest. Dermatol.* **67,** 72–89 (1976).

11. Billingham R.E and SIlvers K. Willys. The Melanocytes of Mammals. *Q. Rev. Biol.* **35,** 1–40 (2012).

12. Seagle, B.-L. L. *et al.* Melanin photoprotection in the human retinal pigment epithelium and its correlation with light-induced cell apoptosis. *Proc. Natl. Acad. Sci. U. S. A.* **102,** 8978–8983 (2005).

13. Ito, S. A Chemist's View of Melanogenesis. *Pigment Cells Res* **16,** 230–236 (2003).

14. D'Ischia, M., Napolitano, A., Pezzella, A., Meredith, P. & Sarna, T. Chemical and structural diversity in eumelanins: Unexplored bio-optoelectronic materials. *Angew. Chemie - Int. Ed.* **48,** 3914–3921 (2009).

15. Tisma, M., Plazl, I., Zelic, B. & Vasic-Racki. Modelling of L -DOPA Oxidation Catalyzed by Laccase. *Chem. Biochem. Eng. Q.* **22,** 307–313 (2008).

16. Beer R. J. S, B. T. and R. A. The Chemistry of the Melanins. Part V . The Autoxidation of 5:6-Dihydroxyindoles. *J. Chem. Soc.* **IV,** 2426 (1954).

17. Arzillo, M. *et al.* Eumelanin buildup on the nanoscale: Aggregate growth/assembly and visible absorption development in biomimetic 5,6-dihydroxyindole polymerization. *Biomacromolecules* **13,** 2379–2390 (2012).

18. Mostert, a. B. *et al.* Role of semiconductivity and ion transport in the electrical conduction of melanin. *Proc. Natl. Acad. Sci.* **109,** 8943–8947 (2012).

19. Panzella, L. *et al.* Atypical structural and pi-electron features of a melanin polymer that lead to superior free-radical-scavenging properties. *Angew. Chemie - Int. Ed.* **52,** 12684–12687 (2013).

20. R. I. T. Cromartie and Mason Harley J. Melanin and its precursors 8. The oxidation of methylated 5:6-dihydroxyindoles. *Biochem. J.* **66,** 713–720 (1957).

21. Pudlas, M. *et al.* Raman Spectroscopy: A Noninvasive Analysis Tool for the Discrimination of Human Skin Cells. *Tissue Eng. Part C Methods* **17,** 1027–1040 (2011).

22. Zhang, G., Moore, D. J., Flach, C. R. & Mendelsohn, R. Vibrational microscopy and imaging of skin: from single cells to intact tissue. *Anal. Bioanal. Chem.* **387,** 1591–9 (2007).

23. Caspers, P. J., Lucassen, G. W. & Puppels, G. J. Combined in vivo confocal Raman spectroscopy and confocal microscopy of human skin. *Biophys. J.* **85,** 572–80 (2003).

24. Huang, Z. *et al.* Raman spectroscopy of in vivo cutaneous melanin. *J. Biomed. Opt.* **9,** 1198–205 (2004).

25. Behbahani, Iraj, Miller A. Sally, O. H. D. A Comparison of Mushroom Tyrosinase Dopaquinone and Dopachrome Assays Using Diode-Arrat Spectrophotometry: Dopachrome Formation vs Ascorbate-Linked Dopaquinone Reduction. *Microchem. J.* **47,** 251–260 (1993).

26. J. Pawelek, Korner, B. and J. B. New regulators of melanin biosynthesis and the autodestruction of melanoma cells.pdf. *Nature* **286,** 617–619 (1980).

27. Foster, M. Non-Enzymatic Oxidation of Tyrosine and DOPA. *Proc. Natl. Acad. Sci.* **36,** 606–611 (1950).

28. Nighswander-Rempel, S. P. *et al.* Effect of dimerization on vibrational spectra of eumelanin precursors. *Photochem. Photobiol.* **84,** 613–619 (2008).

29. Tsukamoto, K., Jackson, I. J., Urabe, K., Montague, P. M. & HEARING, V. J. A 2nd Tyrosinase-related protein, Trp-2, is a melanogenic enzyme termed dpachrome tautomerase. *EMBO J.* **11,** 519–526 (1992).

30. Gauden, M. *et al.* Ultrafast excited state dynamics of 5,6-dihydroxyindole, a key eumelanin building block: nonradiative decay mechanism. *J. Phys. Chem. B* **113,** 12575–12580 (2009).

31. IUPAC. Isosbetic Point. *PAC* **79,** 293 (2007).

32. Croce, a E. First-order parallel and consecutive reaction mechanisms — Isosbestic points criterium. *Can. J. Chem.* **86,** 918–924 (2008).

33. Okuda Hidekazu, Nakamura Atsushi, Wakamatsu Kazumasa, I. S. and S. T. Mid-infrared absorption spectrum of 5,6-dihydroxyindole-2-carboxylic acid. *Chem. Phys. Lett.* **433,** 355–359 (2007).